LAWRENCE
LIVERMORE
NATIONAL
LABORATORY

LLNL-JRNL-425029

# TRISO-Fuel Element Performance Modeling for the Hybrid LIFE Engine with Pu Fuel Blanket

P. DeMange, J. Marian, M. Caro, A. Caro

March 3, 2010

Journal of Nuclear Materials

## Disclaimer

# TRISO-Fuel Element Performance Modeling for the Hybrid LIFE Engine with Pu Fuel Blanket

P. DeMange, J. Marian, M. Caro, A. Caro.
*Lawrence Livermore National Laboratory, Livermore, CA 94551*

## Abstract

A TRISO-coated fuel thermo-mechanical performance study is performed for the hybrid LIFE engine to test the viability of TRISO particles to achieve ultra-high burnup of a weapons-grade Pu blanket. Our methodology includes full elastic anisotropy, time and temperature varying material properties for all TRISO layers, and a procedure to remap the elastic solutions in order to achieve fast fluences up to $30\times10^{25}$ n·m$^{-2}$ ($E$>0.18 MeV). In order to model fast fluences in the range of $\approx7\sim30\times10^{25}$ n·m$^{-2}$, for which no data exist, careful scalings and extrapolations of the known TRISO material properties are carried out under a number of potential scenarios. A number of findings can be extracted from our study. First, failure of the internal pyrolytic carbon (PyC) layer occurs within the first two months of operation. Then, the particles behave as BISO-coated particles, with the internal pressure being withstood directly by the SiC layer. Later, after 1.6 years, the remaining PyC crumbles due to void swelling and the fuel particle becomes a single-SiC-layer particle. Unrestrained by the PyC layers, and at the temperatures and fluences in the LIFE engine, the SiC layer maintains reasonably-low tensile stresses until the end-of-life. Second, the PyC creep constant, $K$, has a striking influence on the fuel performance of TRISO-coated particles, whose stresses scale almost inversely proportional to $K$. Obtaining more reliable measurements, especially at higher fluences, is an imperative for the fidelity of our models. Finally, varying the geometry of the TRISO-coated fuel particles results in little differences in the scope of fuel performance. The mechanical integrity of 2-cm graphite pebbles that act as fuel matrix has also been studied and it is concluded that they can reliable serve the entire LIFE burnup cycle without failure.

## Motivation

The hybrid version of the LIFE (Laser inertial fusion-fission energy) engine provides an attractive pathway to burn fissile materials such as excess weapons-grade Pu (WG-Pu), which can be burnt up to 99% FIMA (fraction of initial metal atoms) in less than a decade of operation [Moses2009]. The LIFE concept being pursued at Lawrence Livermore National Laboratory (LLNL) consists of a point source of 14-MeV neutrons produced by an inertial-confinement fusion engine enveloped by a Be neutron multiplier and a sub-critical fuel blanket. A schematic view of the LIFE engine configuration is shown in Figure 1. Details about the geometry and the neutronic and thermal-hydraulic performance of the reactor have been given by Abbott *et al.* [Abbott2009].

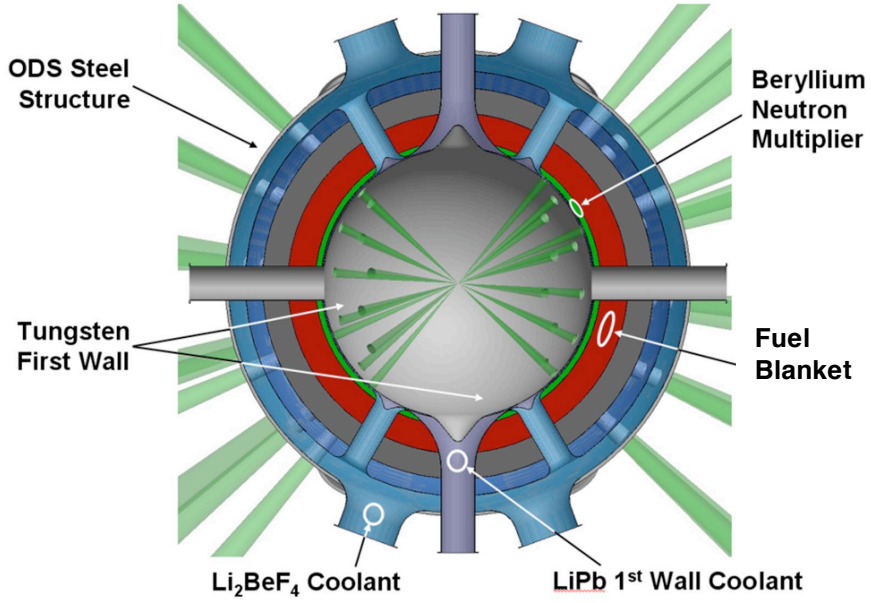


Figure 1: LIFE engine configuration showing the location of the fuel blanket. For the specific dimensions of the reactor, see [Abbott2009].

The type of fuel to be used in the hybrid LIFE engine is still open to debate, including whether it should be in a liquid or solid form. The nominal engine design calls for 2-cm-diameter graphite pebbles containing ≈1-mm-diameter TRISO (TRI-structural ISOtropic) fuel particles suspended in liquid $Li_2BeF_4$ ('flibe') [Abbott2009]. A TRISO particle consists of an internal fuel kernel surrounded by a low-density pyrolytic carbon (PyC) buffer layer to moderate fission product recoils. The buffer layer is coated successively by an inner high-density PyC layer (iPyC), a thin SiC film, and an outer PyC (oPyC). The configuration of a TRISO particle, with its different constituent layers is shown in Figure 2. The preliminary fuel composition for the WG-Pu engine consists of 20% of Pu oxycarbide (PuCO) embedded in a ZrC matrix (80%). The main objective of this paper is to model TRISO-coated fuel particles under LIFE's conditions using the state of the art in fuel performance modeling, and assess the feasibility of TRISO-coated fuel for LIFE's WG-Pu engine.

Next, we review the TRISO-coated fuel performance modeling literature and discuss its suitability for LIFE.

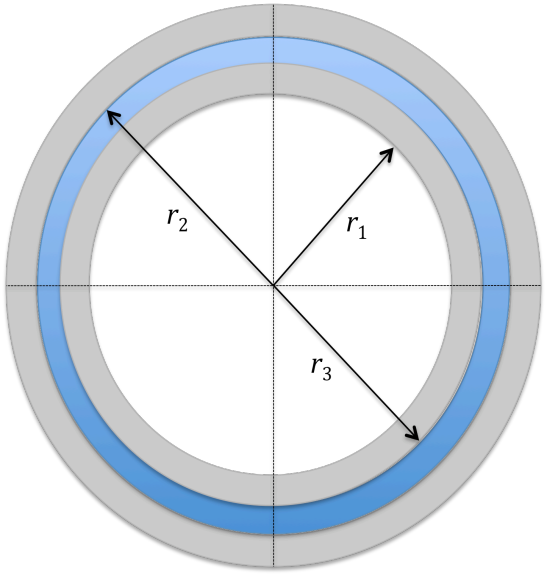


Figure 2: Schematic view of a TRISO particle with its constituent layers. Gray for PyC and blue for SiC. Within the inner PyC layer lie the buffer layer and fuel kernel. The total diameter of the particle is about 1 mm. The specific dimensions of each layer ($r_1$, $r_2$ and $r_3$) are given in the Results section.

## Background

Underwritten by more than three decades of research, mostly in the context of the high-temperature gas-cooled reactor (HTGR) program [Homan1978], TRISO-coated fuel performance modeling has become a critical element in the design of high-temperature fast reactors. In the initial finite-difference models by Walther [Walther1972], Bongartz [Bongartz1979], and Martin [Martin1973], the PyC layers were assumed to undergo irradiation-induced creep and swelling, with negligible elasticity, whereas the SiC layer was assumed to be rigid and not affected by irradiation. These assumptions were justified by the low swelling and creep exhibited by SiC at high temperatures, and by the fact that the elastic modulus of SiC is an order of magnitude higher than that of PyC. In addition, these simplifications were motivated by the need to perform a large number of calculations to obtain failure probabilities, which were costly to calculate with the computing resources of the 1970s.

The full elastic behavior of the TRISO layers can be readily simulated using finite-element codes, such as ABAQUS [abaqus], although simulations of this type are even costlier than finite-difference calculations. Bennet carried out a one-dimensional ABAQUS study of ideal TRISO particles [Bennet1991], being the first one to note that "IPyC and OPyC stresses both exceed the 160-MPa mean fracture stress of PyC" in nominal HTGR particles, and that particles with smaller curvature (e.g. decreased buffer layer thickness) are expected to fail during service due to the rupture of the SiC layer. This finite-element solution was subsequently used by Miller and Bennett [Miller1993] to validate their stress and displacement closed

form solutions for TRISO-coated fuel particles, which include elastic and inelastic (swelling, creep) behaviors, and are formulated as power series in time. This work is essentially what constitutes the basis of the PARFUME fuel performance code [Miller2002, Miller2004].

Miller *et al.* have recently presented updated solutions for isotropic TRISO particles, also benchmarked against ABAQUS results, which include time-dependent material properties [Miller2008]. This is now a standard feature of other fuel performance codes, such as TIMCOAT [Wang2004a, Wang2004b], which uses the solutions developed by Miller and Bennett [Miller1993] and incorporates the full thermo-mechanical and failure-probability analyses for TRISO coated fuel particles in both pebble-bed and prismatic configurations. Another code based on the same time series solution is PASTA [Boer2008], which possesses the extended capability of computing TRISO stresses in the context of the other TRISO particles in the graphite matrix and the matrix itself. By contrast, a full finite-element methodology aimed at quantifying the failed particle fraction and fission product release in normal and accidental conditions has been developed in France [ATLAS]. For a review of most qualified coated-particle fuel performance models, see Liu *et al.* [Liu2007].

All these methodologies are based on perfect axisymmetric geometries (angular symmetry), and elastic isotropy, even for the PyC layers (in contrast to inelastic processes, such as swelling or creep, which are modeled anisotropically). Breaking the angular symmetry, e.g., to simulate the effect of pre-existing cracks, gaps between layers (debonding), local thinning, etc., in the TRISO layers, requires the use of finite-element simulations [Miller2002, Miller2003, Miller2004, Miller2006, Miller2008]. As noted above, these simulations are costly and arbitrary in the sense that flawed geometries are input *ad hoc*, although they are valuable in providing interesting insights beyond the nominal behavior of TRISO-coated particles. Indeed, post-irradiation examinations (PIE) suggest that asymmetric imperfections are responsible for most of the particle failures, at least in US irradiation campaigns [Miller2004].

Despite all these advancements, the use of TRISO fuel for the LIFE engine presents a distinct number of challenges, most notably the extension to very high fast fluences. Fast fluences in the studies mentioned above are typically limited to those expected in HTGR, of the order of $3\times10^{25}$ n·m$^{-2}$ (>0.18 MeV), as specified in the TRISO-Coated Particle Fuel Performance Benchmark developed at Idaho National Laboratory and sponsored by IAEA's Coordinated Research Program [IAEA2005]. By contrast, the fast fluence to achieve 99% burn-up in LIFE's WG-Pu engine is $3.1\times10^{26}$ n·m$^{-2}$ (>0.18 MeV)[1]. Although fuel pebbles are expected to undergo extraction/inspection/recirculation —and thus not being exposed to aggregate fluences as high as the full burn-up fluence—, a fast neutron dose of $3\times10^{25}$ n·m$^{-2}$ corresponds only to 221 days or ≈12% FIMA in LIFE. It is therefore desirable to model longer-term behavior to establish the suitability of TRISO-coated fuel for the hybrid LIFE engine.

[1] Other measures of fast fluence are: $3.61\times10^{26}$ n·m$^{-2}$ (>0.1 MeV), and $1.55\times10^{26}$ n·m$^{-2}$ (>1.0 MeV).

A major hurdle for such modeling, however, is the lack of material property data as a function of neutron dose above the mentioned limit. Moreover, the existing data suffers from a large degree of uncertainty and variability. The reference database for PyC properties under irradiation is that compiled by CEGA over 25 years since the 1970s [CEGA]. Martin has pointed out the major issues regarding the uncertainties in the behavior of PyC under irradiation [Martin2002]. For SiC, due to its interest for fusion applications, more recent data exist [Snead2007].

Here we present a fuel performance study of TRISO-coated particles and fuel pebbles for the LIFE engine. Our method is an extension of the closed-form time series solution of Miller and Bennett to: (a) ultra high fast fluences ($\sim 30\times10^{25}$ n·m$^{-2}$, $E$>0.18 MeV); (b) radial and time dependent material properties; (c) elastic anisotropy, and (d) an arbitrary number of layers. Our calculations hinge on judicious extrapolations to very high fluences of the known properties of PyC and SiC under irradiation. First, we provide some operational information about the WG-Pu LIFE engine and the material properties used. Then, a brief theoretical overview is given, followed by results for nominal and LIFE TRISO geometries. Specifically, we calculate layer stress buildup considering all the features enabled by our model extension (see (a) to (d) above), and varying the creep constant given the large uncertainty and importance of this parameter. We finalize with the discussion and the conclusions.

## Preliminaries

### LIFE Boundary Conditions.

The WG-Pu LIFE engine design contemplates a 77-cm-thick fuel blanket containing fuel elements consisting of approximately 2444 TRISO particles embedded in 2-cm-diameter graphite pebbles circulating in flibe [Abbott2009]. The fuel blanket has a 30% TRISO packing fraction and a 0.58 fuel-to-moderator ratio. For 500 MW of fusion power, the fuel blanket is envisioned to have $\approx1.32\times10^{7}$ pebbles, which provide a multiplication factor of 7.6 for a total thermal power of 3,800 MW. The thermal power begins immediately at full power (3800 MW) because at startup the system has the highest fissile content and is in the most critical configuration, even though it is still subcritical. Fissile consumption continues up to ≈80% FIMA (4.5 years), at which point, there is a six-fold reduction in thermal power to about 600 MW. It takes approximately another five years to completely incinerate the heavy metal content to 99% FIMA. Under these conditions, the innermost pebbles experience the highest temperatures, with surfaces at 700°C and an average volumetric nuclear heating of 130 W·cm$^{-3}$ at full power [Kramer2009]. The pressure accumulated in a TRISO particle due to gaseous fission products (mostly Kr and Xe) as a function of burn-up and time is shown in Figure 3. We have calculated the gas pressure due to transmutation He and H in the kernel and found it to be negligible ($10^{-3}$ times that of the fission products). Here we assume that the buffer layer presents no barrier to the fission gases. Therefore, Figure 3 provides the internal boundary condition for the TRISO-fuel calculations.

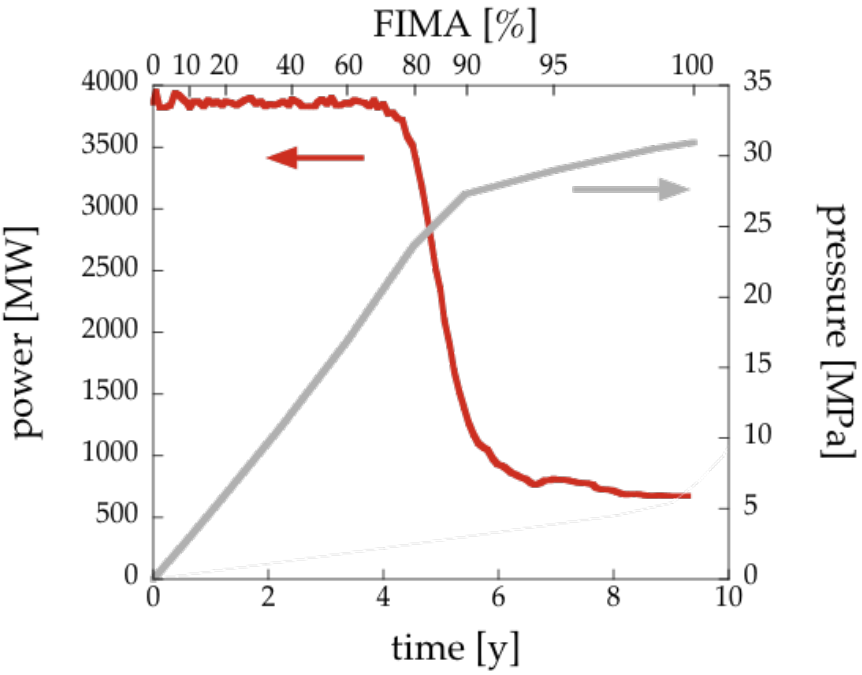


Figure 3: In red, 3800 MWth (WG-Pu) LIFE engine power as a function of time (and FIMA). In gray is the corresponding fission gas buildup in a TRISO kernel. Note the change in slope for the pressure buildup when the Pu inventory is consumed at approximately 80% FIMA.

Figure 4a shows the energy spectra of the total flux in the fuel blanket at different burn-ups. We emphasize that, in the WG-Pu engine, the highest fissile content occurs at the time of startup. Thus, the characteristic thermal peak in the neutron spectrum does not exist due to the high fuel-to-moderator ratio at BOL[2]. As the Pu concentration in the fuel decreases with burn-up, and fission products build up, the spectrum becomes softer leading also to the presence of a Maxwellian at high FIMA (>80%) [Kramer2009]. Except for the unaltered fusion peak at ≈14 MeV, the fast fluence increases only marginally thereafter. At this time, the pulsed nature of the LIFE engine is not taken into account, as preliminary studies suggest that its effect is negligible in the fuel blanket [Abbott2008]. Figure 4b shows the total and fast fluences as a function of time in the LIFE engine. Regardless of the measure used, the fluence in LIFE is close to an order of magnitude larger than the most severe high burn-up concepts, such as the VHTR (Very High Temperature Reactor, a Generation IV concept) [Maki2007]. This fact defines the nature of our study, in the sense that the behavior and evolution of TRISO-fuel materials must be extrapolated to levels that are impossible to verify with existing data. We can only go as far as using our best judgment to predict upper and lower bounds for the existing trends, and defining fuel performance in this range. In what follows, we provide the materials behavior laws used in this work, as well as the reasoning behind the

[2] BOL: beginning of lifetime; EOL: end of lifetime.

extrapolation approximations adopted.

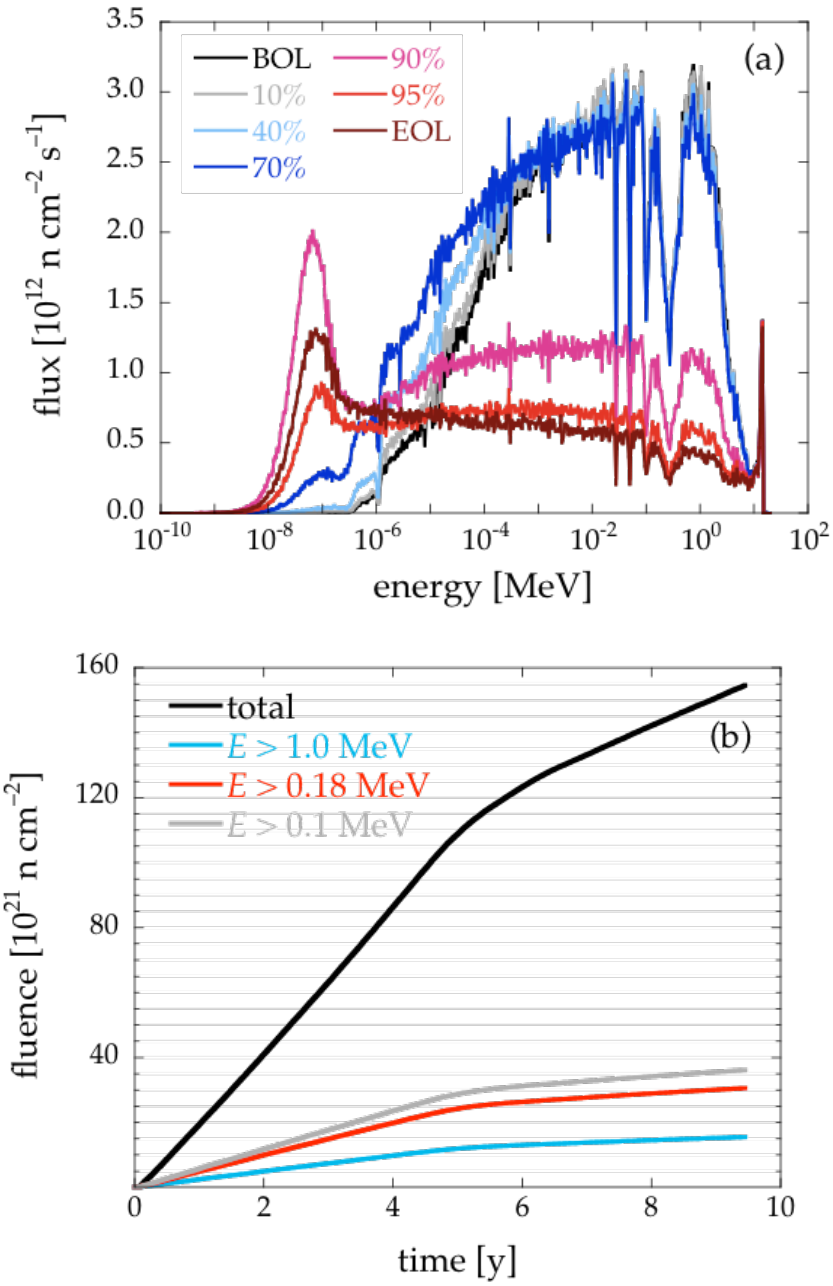


Figure 4: (a) Total neutron flux at different burn-ups in the WG-Pu LIFE engine. Note the fusion peak at approximately 14 MeV for all cases and the development of a thermal (Maxwellian) distribution at high burn-ups. (b) Total and fast fluences as a function of time.

Under these circumstances, the damage parameters obtained using the SPECTER code [Marian2009] for several relevant materials in the fuel blanket are given in **Table 1**. These values are very high and, as we shall see below, in some cases there exist no experimental data that can even suggest materials behavior in this range. However, if we look at the results in terms of damage per full power year

(pfy), we see that the rates are even below what can be achieved in current or past test reactors, such as HFIR (28 and 33 dpa/efpy for SiC and Fe, respectively), ATR (12 and 14), EBR-II (27 and 25), and FFTF (53 and 48) [Heinisch2002].

Table 1: Displacement damage and gas production in several relevant materials in LIFE's WG-Pu fuel blanket. Numbers in parenthesis are damage and gas production rates given per full power year (fpy).

| Material | Si | C | Zr | Fe |
|---|---|---|---|---|
| Total dpa | 48 | 31 | 28 | 26 |
| (dpa rate) | (5.1) | (3.3) | (3.0) | (2.8) |
| Total He | 351 | 1073 | 10 | 70 |
| (He rate) | (37.4) | (114.1) | (1.1) | (7.4) |
| Total H | 624 | 15 | 48 | 338 |
| (H rate) | (66.4) | (1.6) | (5.1) | (36.0) |

## Theory.

The general constitutive equations for a spherical layer in reduced tensor notation are:

$$\varepsilon_l = \sum_{m=1}^{3}\left[E_{lm}\sigma_m + K_{lm}\sigma_m\phi t + C_{lm}\sigma_m^n t\right] + \alpha_l T + S_l(\phi t) \quad (l=1,3) \qquad (1)$$

where $l$=1,2 refers to mutually orthogonal tangential directions and $l$=3 is the radial direction. Here, $\sigma$, $\phi t$, and $T$ are the stresses, fast neutron dose, and absolute temperature, and $E$, $K$, and $C$ are the elastic, irradiation creep and thermal creep constants. The constants relating strains with temperature are the thermal expansion coefficients $\alpha$, and the $S$ are the irradiation-induced dimensional changes. For axisymmetric solids, the two tangential directions are equivalent[3], which we now represent by $l$=1, and the material property tensors are:

$$\mathbf{E} = \begin{bmatrix} \frac{1}{E_1} & -\frac{\mu_{11}}{E_1} & -\frac{\mu_{13}}{E_1} \\ -\frac{\mu_{11}}{E_1} & \frac{1}{E_1} & -\frac{\mu_{13}}{E_1} \\ -\frac{\mu_{31}}{E_3} & -\frac{\mu_{31}}{E_3} & \frac{1}{E_3} \end{bmatrix} \quad \mathbf{K} = \begin{bmatrix} \frac{1}{K_1} & -\frac{\nu_{11}}{K_1} & -\frac{\nu_{13}}{K_1} \\ -\frac{\nu_{11}}{K_1} & \frac{1}{K_1} & -\frac{\nu_{13}}{K_1} \\ -\frac{\nu_{31}}{K_3} & -\frac{\nu_{31}}{K_3} & \frac{1}{K_3} \end{bmatrix} \quad \mathbf{C} = \begin{bmatrix} \frac{1}{C_1} & -\frac{\nu_{11}}{C_1} & -\frac{\nu_{13}}{C_1} \\ -\frac{\nu_{11}}{C_1} & \frac{1}{C_1} & -\frac{\nu_{13}}{C_1} \\ -\frac{\nu_{31}}{C_3} & -\frac{\nu_{31}}{C_3} & \frac{1}{C_3} \end{bmatrix}$$

where $\mu$ and $\nu$ are, respectively, the elastic Poisson ratios and the Poisson ratio in creep. $E_1$ and $E_3$ are the shear modulus and the Young's modulus, while $K$ and $C$ are usually temperature and material density dependent, but typically not fluence or time dependent. In most practical scenarios, the irradiation and thermal creep constants are obtained for a single stress state and anisotropic data is quite scarce. This simplifies the number of terms associated with $K$ and $C$ in eq. (1). Closure of eqs. (1) is achieved via the equilibrium equation:

[3] All off-diagonal components, corresponding to shear strains and stresses, are identically zero.

$$\sigma_1 = \sigma_3 + \frac{r}{2}\frac{d\sigma_3}{dr} \qquad (2)$$

and the definition of the strains as a function of the displacements, which in axisymmetric geometries using spherical coordinates can be expressed simply as a function of the radial displacement *u*:

$$\begin{aligned} \varepsilon_1 &= \frac{u}{r} \\ \varepsilon_3 &= \frac{du}{dr} \end{aligned} \qquad (3)$$

Following the work of the PARFUME group [Miller2002, Miller2004, Boer2008], the displacements and the radial and tangential stresses are assumed to be well represented by power series of the form:

$$\begin{aligned} u(r,t) &= \sum_{i=0}^{\infty} u_i(r)t^i \\ \sigma_l(r,t) &= \sum_{i=0}^{\infty} \sigma_{li}(r)t^i \end{aligned} \qquad (4)$$

Combining eqs. (1)-(4), and assuming that the thermal creep exponent *n*=1, we obtain an Euler-Cauchy type equation in *u* with one real double root (see the Appendix for the full derivation). Retaining the full anisotropy in the equations leads to solutions of the type:

$$\sigma_{li}(r) = \sum_{j=0}^{i}(A_{lj}r^p + B_{lj}r^q)Log(r)^j + \sum_{\substack{\tau=-1 \\ \tau\neq 1}}^{2} C_{li\tau}r^\tau \qquad (5)$$

where, again, *l*=1, 3, and

$$p = -\frac{3}{2} + \frac{1}{2}\sqrt{1 + \frac{8(1-\mu_{13})}{(1-\mu_{11})}\frac{E_1}{E_3}}, \quad q = -\frac{3}{2} - \frac{1}{2}\sqrt{1 + \frac{8(1-\mu_{13})}{(1-\mu_{11})}\frac{E_1}{E_3}} \qquad (6)$$

The *A, B,* and *C* are recursive coefficients obtained by applying the boundary conditions introduced at each $i^{th}$ iteration by the $t^i$ dependence of the time-dependent properties (swelling, creep, temperature, and fission pressure). To account for higher order dependence of the elastic constants on fluence, the stress calculation code contains a remapping algorithm. At fluence intervals $\Delta t$, over which the quadratic approximation remains accurate, the stresses are restarted using the functional form corresponding to *t*=0 and re-inserted as the *i*=0 term into the power series solution. New quadratic approximations to the elastic constants for the next $\Delta t$ fluence interval are then obtained. As such, the solution for the stresses at high fluence is a piecewise function of finite powers series solutions over $\Delta$t fluence intervals. Determining the optimum length of $\Delta t$ is a numerical process that depends

on the time-dependent material properties and requires some degree of trial and error.

### Material properties.

There exists a considerable volume of literature on material properties for PyC and SiC dating back to the 1950s. Much of this knowledge is empirical and valid only in the context of the technique or facility used to carry out the experiment, and many uncertainties still remain. In particular, the fluence dependence of the material properties is critical to make sound assessments of the thermo-mechanical behavior of TRISO-coated particles under irradiation. Evidently, no data exist in the range of conditions given above for the LIFE engine, which forces us to make extrapolations into the required ranges. In what follows, we justify the extrapolations adopted and provide a comprehensive set of material parameters for both PyC and SiC.

Regarding PyC, the most authoritative source of experimental data is the CEGA database [CEGA], compiled in 1993 from studies carried out over the last several decades. For example, PyC layers can develop some degree of anisotropy during the deposition process, which affects elastic properties and irradiation induced dimensional changes. Anisotropy is quantified at BOL by the Bacon Anisotropy Factor ($BAF_0$) [Bacon1956], taken to be 1.0342 and 1.0256 for iPyC and oPyC, respectively[4]. All the material properties used in this work correspond to a pyrocarbon density of $\rho$ =1.85 g·cm$^{-3}$ and are given in **Table 3**. The irradiation swelling and creep relations deserve special attention. Swelling data up to 7.7×10$^{25}$ n·m$^{-2}$ (>0.18 MeV) exist from a number of sources [Kaae1971, Kaae1972, Kaae1974, Kaae1975, CEGA, INEEL2004]. These measurements show that dimensional changes along the radial direction have a 'parabolic' dependence with fluence, with an initial shrinkage due to PyC densification followed by unbounded swelling. On the other hand, along the tangential direction, the evidence points to continued shrinkage up to fast fluences of 5×10$^{25}$ n·m$^{-2}$. These data are typically fitted to third-order polynomials that capture the large variability often observed in the experimental measurements [Wang2004c, IAEA2005]. However, these are not suitable for extrapolation up to an order-of-magnitude higher fast fluences. Exponential fits, such as those used for the German AVR [INEEL2004] are more appropriate for extrapolation, as they remain monotonic in the entire fluence range. However, it is impossible to know if a given trend will persist throughout an entire order of magnitude in fluence. It is probably reasonable to assume that radial swelling will continue to increase as a function of fluence. However, tangential shrinkage is unlikely to continue indefinitely, for material densification eventually saturates and a new phase starts —akin to the radial case— characterized by unrestrained swelling. Consequently, here we consider that the tangential swelling behaves as the radial swelling —*i.e.* initial densification followed by unrestrained swelling—, albeit with a densification peak shifted to higher fluences. In this scenario, the existing

[4] These values were provided by Babcock & Wilcox in a batch of TRISO-coated particles fabricated for experimental testing at LLNL.

experimental data in the tangential direction simply captures the initial densification stage, with the peak's position being unknown.

The procedure to fit PyC dimensional changes to the swelling regime is as follows. PyC swelling curves as a function of fluence for different initial BAF values and irradiation temperatures have been reported [INEEL2004, Wang2004c]. From the values corresponding to a *BAF* of 1.036 (the closest to our manufactured particles), we use those at 600°C and 1050°C (between which our operating temperature of ≈700°C falls) and perform the following quadratic least-squares fit in fluence:

$$S_1(T,\phi t) = a(T)(\phi t)^2 + b(T)(\phi t) \qquad (7)$$

This results in the fit coefficients given in **Table 2**:

Table 2: Radial and tangential strain coefficients stemming from a quadratic fit (eq. (7)) of PyC swelling data for *BAF*=1.036 at 600 and 1050°C.

| Radial Strain (%) | | | Tangential Strain (%) | | |
|---|---|---|---|---|---|
| $T$ [°C] | $a$ | $b$ | $T$ [°C] | $a$ | $b$ |
| 600 | 0.153 | −1.044 | 600 | 0.141 | −1.276 |
| 1050 | 0.280 | −1.145 | 1050 | 0.139 | −1.493 |

We next ascribe a linear temperature dependence to $a$ and $b$ to obtain swelling laws at 700°C. The resulting relations are:

$$S_1(\phi t) = 0.140(\phi t)^2 - 1.324(\phi t)$$
$$S_3(\phi t) = 0.181(\phi t)^2 - 1.066(\phi t) \qquad (8)$$

These relations and the data points at 600 and 1050°C are shown in Figure 5. One can see that, for example, the maximum densification along the tangential direction now occurs at $4.8\times10^{25}$ n·m$^{-2}$, which means that studies done below this point capture only the shrinking phase of PyC. Subsequently, densification ceases and the material starts to swell up to the breakage point. Since PyC is quite permeable to He gas [Bullock1980], we have not scaled these curves to the LIFE He production to account for fast flux effects.

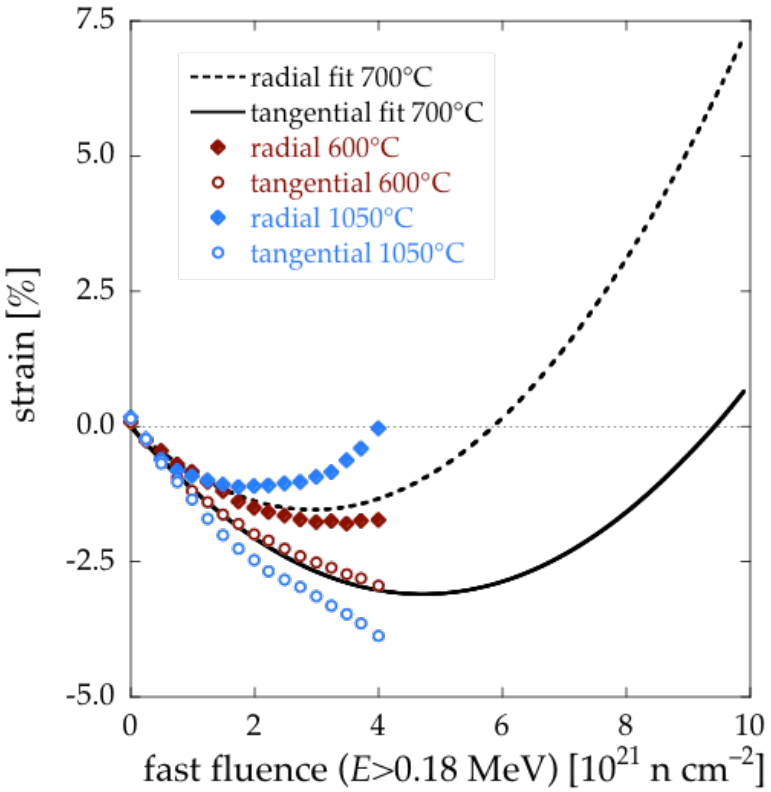


Figure 5: Quadratic extrapolation of the radial and tangential swelling laws for PyC under fast neutron irradiation.

We emphasize that this behavior is speculative, but it represents an upper bound to the total PyC swelling, which is helpful to delimit the TRISO stress evolution. It will also be assumed that PyC breakage occurs at 30% volumetric swelling regardless of the internal stress state. The true volumetric swelling is:

$$S_v = 2S_1 + S_3 + S_1^2 + 2S_1S_3 + 2S_1^2S_3 \qquad (9)$$

Assuming small deformations, *i.e.* neglecting terms of order two and higher in eq. (9)[5], $S_v$=0.3 is reached at a fast fluence of $8.14\times10^{25}$ n·m$^{-2}$.

With respect to creep, we only consider secondary irradiation creep, as there are no experimental measurements of primary creep and Miller has shown that its effect is marginal for a broad range of values [Miller1995]. Here we utilize the data and creep relations obtained by General Atomics starting in the late 1960s [Prados1967, Kaae1971, Kaae19782, Brocklehurst1976]. A value of 0.5 is usually used for the Poisson's ratio in creep, $\nu_c$, although lower values have also been considered [Kaae1971]. The evolution of $\nu_c$ with irradiation and/or anisotropy is not clear but it is typically accepted that its value decreases with fluence.

Table 3: PyC material properties used in stress calculations.

| Parameter [units] | Value and/or correlation used | Notes | Source |
|---|---|---|---|

[5] Which results in errors of approximately 10%

| | | | |
|---|---|---|---|
| Coefficient of thermal expansion [$\times 10^{-6}$ K$^{-1}$] | $\alpha_1 = \alpha_3 = 5.5$ | Assumed unchanged with irradiation | [INEEL2004] |
| Thermal conductivity [W m$^{-1}$ K$^{-1}$] | $k = 16.0$ | | [Lopez2008, Basini2005] |
| Anisotropic orientation parameters | $R_1 = \frac{2}{2 + BAF_0}$ and $R_3 = \frac{1 - R_1}{2}$ | For isotropic PyC $R_1$=$R_3$. | [CEGA] |
| Young's modulus [MPa] | $E_l = k_\rho k_L k_\phi k_T k_{BAF_0} E_0$<br>$E_0 = 39600$<br>$k_\rho = 0.384 + 0.324\rho$<br>$k_L = 2.985 - 0.662L$<br>$k_\phi = 1 + 0.23\phi t$<br>$k_T = 1 + 0.00015(T - 20)$<br>$k_{BAF_0} = \begin{cases} 0.481 + 0.519BAF_0, & l = 1 \\ 1.463 - 0.463BAF_0, & l = 3 \end{cases}$ | $L$ is the characteristic grain size (30~100 Å) and $T$ is the temperature in °C;<br>For isotropic PyC: $E_1$=$E_3$=$E_0$ | [CEGA] |
| Irradiation-induced creep rate [$\times 10^{25}$ MPa n m$^{-2}$]$^{-1}$ | [a] $\dot{\varepsilon}_3 = \dot{\varepsilon}_1 = 8.5 \times 10^{-5}\sigma$<br>[b] $\dot{\varepsilon}_3 = \dot{\varepsilon}_1 = 3.0 \times 10^{-4}\sigma$ | [a]Cases (i) and (iii);<br>[b]Case (ii) | [CEGA, Kaae1972] |
| Poisson's ratio | $\mu_{11} = 0.766R_1 - 0.375$<br>$\mu_{13} = -0.88R_1 + 0.825$<br>$\mu_{31} = \frac{\nu_{13}E_1}{E_3}$ | Relations used in all cases | [CEGA, Price1969] |
| Poisson's ratio in creep | $\nu_{13} = \nu_{31} = \nu_{11} = 0.5$ | Kaae puts it as low as 0.35 [Kaae1971] | [INEEL2004] |
| Irradiation-induced swelling rate [$\times 10^{21}$ n cm$^{-2}$]$^{-1}$ | $\dot{S}_1(\phi t) = -0.0132415 + 0.00280286\phi t$<br>$\dot{S}_3(\phi t) = -0.0106641 + 0.00362582\phi t$ | Based on extrapolation from [Wang2004c] (see text) | |
| Tensile strength [MPa] | ~200 | [Bongartz1976] | |

Regarding SiC, most TRISO-coated fuel performance studies assume that it behaves as an isotropic ideal elastic material (see the Background section above). In this work, however, we test this assumption by making the SiC layer yield by way of irradiation-induced creep and swelling. Snead *et al.* have published a comprehensive compilation of material property data for nuclear applications [Snead2007], which constitutes the main source used in this paper. The values and assumptions used are given in **Table 4**.

Table 4: SiC material properties used in stress calculations.

| Parameter [units] | Value and/or correlation used | Notes | Source |
|---|---|---|---|
| Coefficient of thermal expansion [$\times 10^{-6}$ K$^{-1}$] | $\alpha = 4.9$ | Value at 650°C; Unchanged with irradiation | [Snead2007] |
| Thermal conductivity [W m$^{-1}$ K$^{-1}$] | $k = k_0\left(1 + \exp\{-0.202\phi t\}\right)$<br>$k_0 = 106$ | Correlation extracted from experimental data; $k_0$ is value at 650°C | [Snead2007] |
| Irradiation-induced swelling [$\times 10^{25}$ n m$^{-2}$]$^{-1}$ | $S_l = 0.0008\phi t$ | Linear swelling, scaled to LIFE's fast fluence from data at 600°C | [Blackstone1971, Snead2007] |
| Young's modulus [GPa] | $E = E_0\left(1 - 2.2S_l\right)$<br>$E_0 = 446$ | Correlation extracted from experimental data; $E_0$ is value at 600~700°C | [Snead2007] |
| Irradiation-induced creep rate [$\times 10^{25}$ n m$^{-2}$ MPa]$^{-1}$ | $\dot{\varepsilon}_c = a\sigma^n \exp\{-Q/RT\} + b\sigma$<br>$Q = 2\times 10^5$ [J mol$^{-1}$]<br>$b = 2.7\times 10^{-7}$ [MPa$^{-1}$]<br>$a = 5\times 10^{-6}$ [MPa s]$^{-1}$ | Both thermal and irradiation creep included. From [Nosek2007], $n$=1 | [Snead2007, Nosek2007] |
| Poisson's ratio | $\mu = 0.21$ | Unchanged with irradiation | [Snead2007] |
| Poisson's ratio in creep | $\nu_c$=0.5 | | [Snead2007] |
| Fracture strength [MPa] | ~400 | For CVD SiC | [Snead2007] |

## Results

We have performed calculations on two types of TRISO geometries, namely, the HTR fuel specifications given for the European and US programs for high burn-up TRISO qualification [Phelip2004, Barnes2008], and the driver fuel concept used in deep-burn (DB) reactor-based transmutation [DelCul2002, Rodriguez2003, Talamo2009, Powers2009]. Nominal dimensions for both TRISO-particles are given in **Table 5**. The HTR geometry has been widely used in Germany as part of their HTR spherical fuel-element development and successfully irradiated to FIMA of up to ≈25% [Nickel2002]. It is also the basis for the ATR[6] experimental program for the Advanced Gas Reactor Fuel Development and Qualification in the US, although several differences exist, especially related to the fabrication methodology [Petti2003]. Indeed, several test cases in IAEA's TRISO-Coated Particle Fuel Performance Benchmark [IAEA2005] are built around this geometry. For its part,

[6] Advanced Test Reactor, at Idaho National Laboratory (http://atrnsuf.inl.gov).

for DB transmutation, kernels of large diameter compared to the resonance mean free path must be used, to enhance self-shielding and maximize fission capture versus absorption [Rodriguez2003]. In addition, Pu kernels are known to produce a higher fraction of metallic fission products, such as Pd and Ag, which may result in higher levels of chemical attack to the SiC coating [INEEL2002, Harding2004]. This advises using thicker SiC coatings as a preventive measure. By maintaining the same fuel-to-moderator ratio of 0.58 in the LIFE engine, these dimensions also determine the size of the graphite pebbles to be used. Therefore, as **Table 5** shows, the main differences reside in the kernel diameter, the buffer thickness, and the SiC layer thickness.

Table 5: Geometry of TRISO-coated particle fuel for the HTR program used in previous experiments and LIFE fuel particles fabricated by BWX.

| Layer | HTR | DB |
|---|---|---|
| Kernel diameter (μm) | 500 | 640 |
| Buffer thickness (μm) | 95 | 100 |
| Inner PyC thickness (μm) | 40 | 40 |
| SiC thickness (μm) | 35 | 45 |
| Outer PyC thickness (μm) | 40 | 40 |

Specifically, the three scenarios considered to assess the effect of irradiation, elastic anisotropy, and material properties on the stress evolution on TRISO-coated particles are:

(i) For the HTR geometry, we calculate radial and tangential stresses at the inner surfaces of the iPyC, SiC and oPyC layers up to EOL, including all the time dependencies (given in Tables 1 and 2) and full elastic anisotropy.

(ii) Case (i) is repeated increasing the creep coefficient of PyC from 0.85 to 3.0 $[\times 10^{25}\ \text{n cm}^{-2}]^{-1}$ (Table 1).

(iii) Case (i) is repeated for the DB particle geometry.

We start with cases (i) and (ii) for the HTR geometry, followed by case (iii) for the LIFE-DB design. We assume that the PyC and SiC layers fail at their respective fracture strengths of 200 and 400 MPa (Tables 4 and 5)[7], and that PyC fails at a fast fluence of $8.14\times10^{25}$ n·m$^{-2}$ due to 30% void swelling regardless of its stress state.

### Case (i): HTR TRISO-fuel calculations.

Figures 6, 7 and 8 pertain to case (i) above. Figure 6 shows the tangential stress at the inner radii of the iPyC ($r_1$ in Figure 2), SiC ($r_2$), and oPyC ($r_3$) layers. Tensile tangential stresses develop initially in the PyC layers due to irradiation-induced densification. The slight non-zero stresses at BOL are due to differential thermal expansion. At a fast fluence of $0.46\times10^{21}$ n·cm$^{-2}$, the iPyC coating reaches the fracture strength of PyC of 200 MPa, giving rise to layer fracture. From that point onwards, the fission gas pressure is transmitted to the inner surface of the SiC layer,

[7] We assume that the tensile strength in brittle materials is much lower than the compressive strength and that, thus, these materials do no fail under compression [Wu2002].

resulting in BISO-coated particle behavior. This is seen in Figure 7, where the inner pressure is smoothly transmitted to the SiC layer. Note that this is a conservative assumption, as the sudden breakage of the iPyC layer is likely to result in more available free volume for the fission gases to expand, giving rise to a lower pressure. However, since fracture is a very localized phenomenon, this extra free volume is likely to be negligible. At the beginning of the BISO stage, the SiC and oPyC stresses invert their sign, although the largest effective curvature of the BISO particle makes the inverted stresses to be reduced in magnitude. During the BISO regime, the oPyC reaches the densification peak (with $\sigma_t$ always below 200 MPa) and begins to swell, until, at a fast fluence of $8.14\times10^{25}$ n·m$^{-2}$, it crumbles internally due to void swelling (30% volumetric) and fails. During this stage, the SiC tangential stress becomes tensile up to 196 MPa, well below the adopted tensile strength of SiC given in Table 3. Upon failure of the oPyC layer, the SiC coating is no longer restrained and the tangential stress decreases significantly. Thereon, SiC stresses are simply governed by creep and swelling, which result in a gradual and slow increase in the tensile region up to a value of ≈137 MPa at EOL. At EOL, the calculated SiC swelling is only of 2.6%, very tolerable in terms of thermo-mechanical performance.

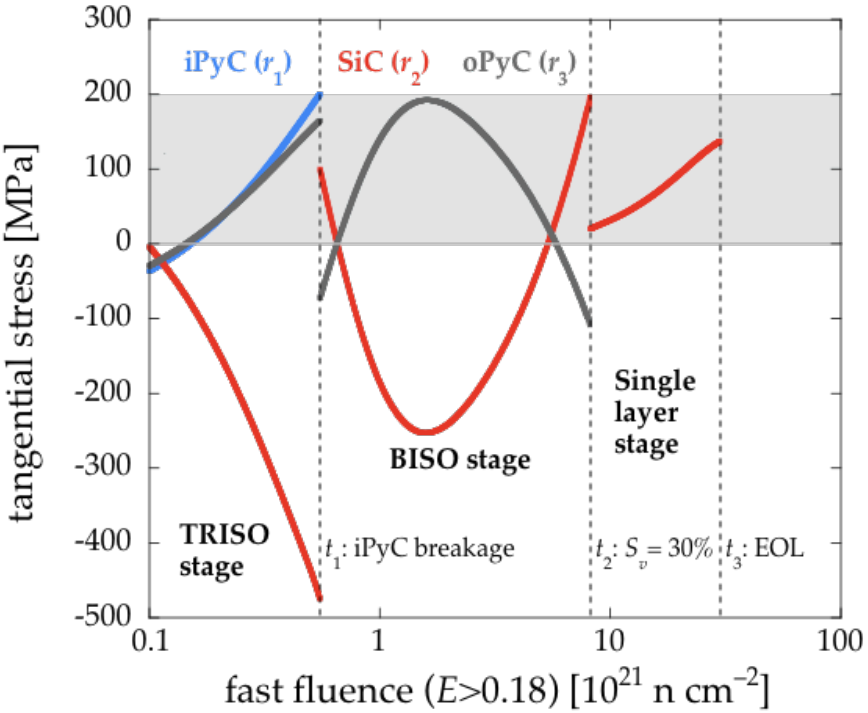


Figure 6: Tangential stress as a function of fast fluence at the inner radii of the iPyC, SiC, and oPyC layers for the HTR case. The three vertical dashed lines mark the times at which, respectively, iPyC failure occurs, oPyC failure occurs, and EOL. In the time intervals delimited by these times, the fuel particle behaves successively as a TRISO, BISO, and single-layer-coated particle. The shaded region represents the tensile stress regime where PyC retains mechanical integrity.

Regarding the radial stresses, during the BISO stage the SiC layer supports the fission gas pressure buildup until EOL, while the oPyC suffers mostly compressive

stresses always well below the de-bonding limit of ≈240 MPa (unirradiated) [Snead2007]. Per Figure 4, $t_1$, $t_2$ and $t_3$ in Figs. 6 and 7 correspond to times of, respectively, 0.2, 1.6 and 9.4 years in the LIFE WG-Pu engine.

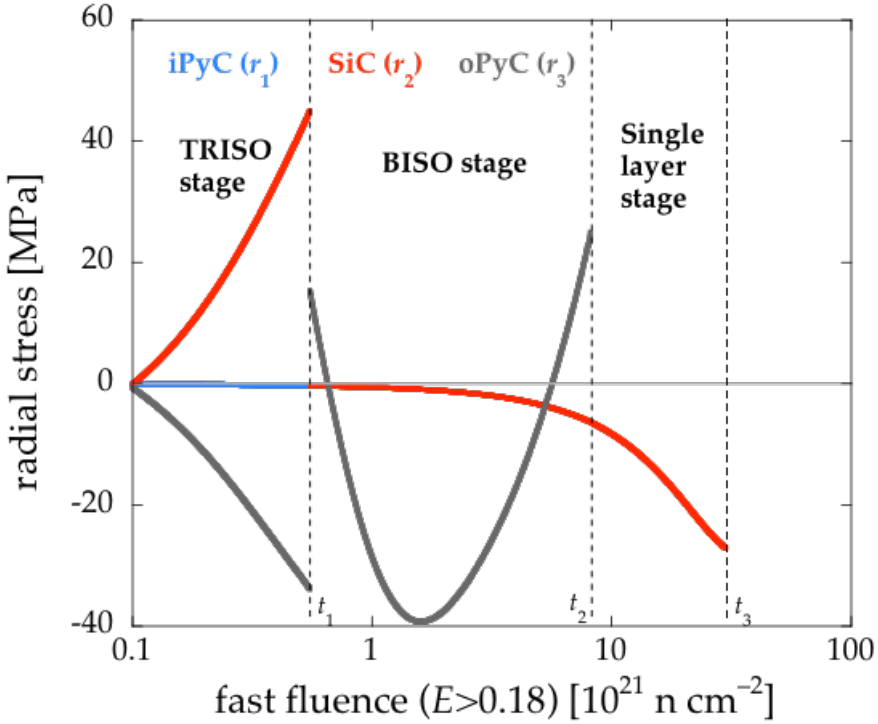


Figure 7: Radial stress as a function of fast fluence at the inner radii of the iPyC, SiC, and oPyC layers for the HTR case.

Figure 8 shows a radial cut of the stresses just before the point of iPyC failure. The radial profile of the particle temperature at the same point in time is also shown. The temperature profile captures the differences in thermal conductivity across the three layers. Interestingly, $\Delta T$ is only one degree from $r_1$ to $r_4$, showcasing that the heat exchange between the center of the particle and the matrix is limited by the thermal conductivity in the kernel and buffer layers. We emphasize that here we are solving the coupled thermo-mechanical problem and, thus, material properties vary radially with temperature.

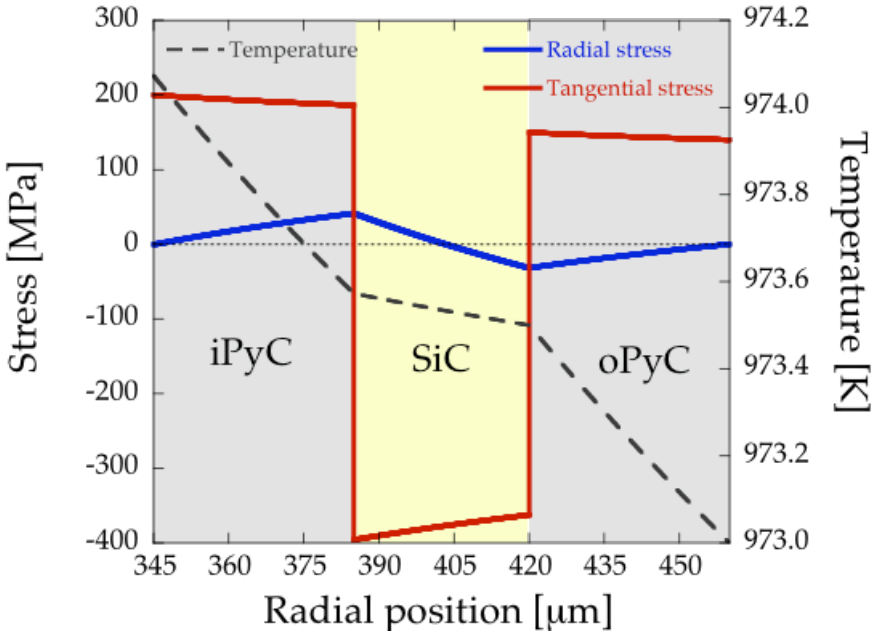


Figure 8: Radial profile of the stress state and temperature inside a TRISO-coated HTR particle for case (ii). The stresses and the temperature correspond to the point of iPyC breakage of 200 MPa at $0.46\times10^{21}$ n cm$^{-2}$. The temperature profile captures the differences in thermal conductivity among the three layers.

### Case (ii): Impact of the creep constant on HTR TRISO-fuel calculations.

As Martin and others have noted [Martin2000], the PyC creep coefficient plays a fundamental role in fuel performance modeling. Figures 9 and 10 show the evolution with fast fluence of the tangential and radial stresses of an HTR particle subjected to LIFE's conditions assuming a PyC creep coefficient of $K$=$3.0\times10^{-4}$ [MPa$^{-1}\cdot(10^{21}$ cm$^{-2})^{-1}$] (as opposed to $K$=$8.5\times10^{-5}$ MPa$^{-1}\cdot(10^{21}$ cm$^{-2})^{-1}$ for case (i) above). A direct comparison with Figs. 6 and 7 reveals that, roughly, the stresses scale directly with the creep coefficient, hence its importance. In fact, neither the iPyC nor the oPyC surpass their strength limit of 200 MPa throughout the reactor's operational cycle, and fail only at a fluence of $8.14\times10^{25}$ n·m$^{-2}$ ($t_1$=1.6 years), when 30% volumetric swelling is reached. This means that the BISO regime does not appear in this case.

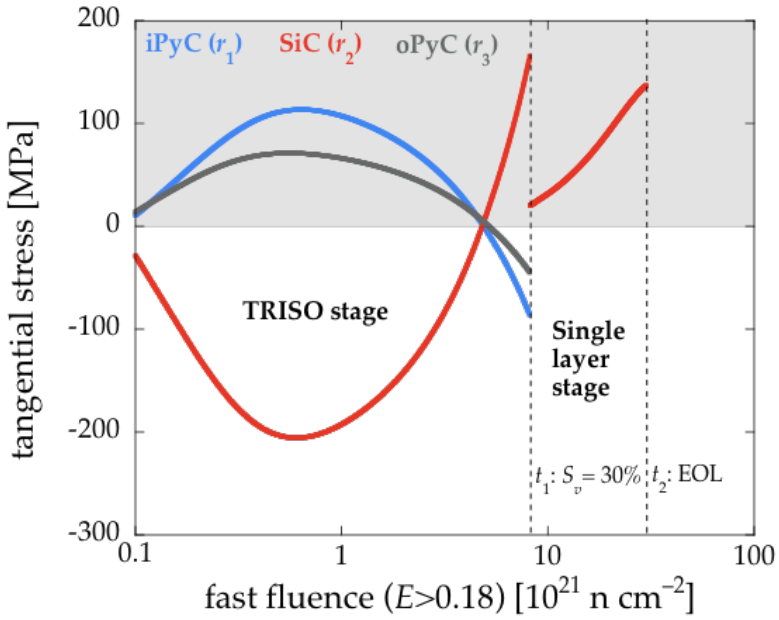


Figure 9: Tangential stress as a function of fast fluence at the inner iPyC, SiC, and oPyC radii for the HTR TRISO-fuel design under case (ii), showcasing the effect of the enhanced PyC creep constant used ($K$=3.0×10$^{-4}$ vs. 8.5×10$^{-5}$ [MPa$^{-1}$·(10$^{21}$ cm$^{-2}$)$^{-1}$] for case (i)).

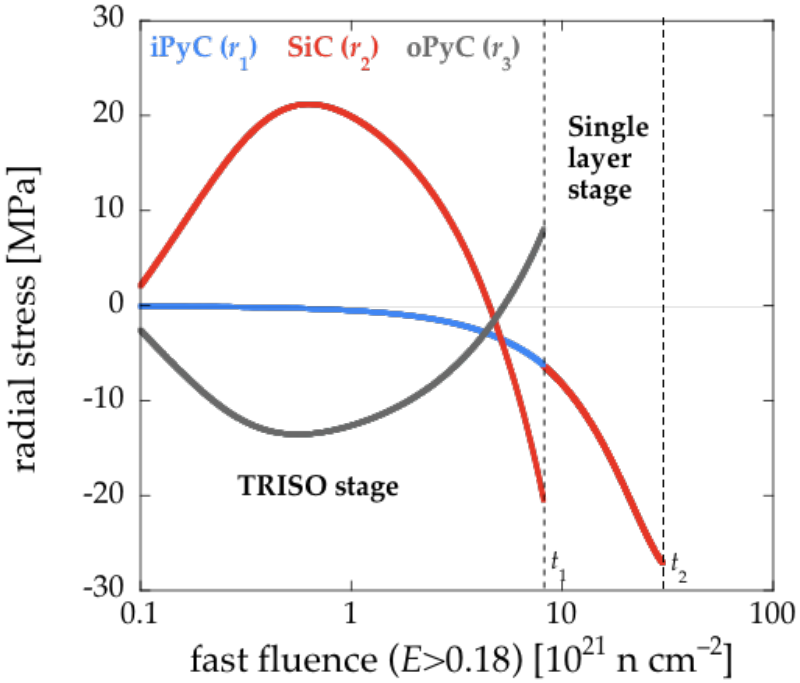


Figure 10: Radial stress as a function of fast fluence at the inner iPyC, SiC, and oPyC radii for the HTR TRISO-fuel design under case (ii).

### Case (iii): Deep burn TRISO-fuel calculations.

The calculations for the deep burn geometry are shown in Figs. 11 and 12. Despite the difference in kernel and layer sizes, we have used the same internal pressure boundary condition as in the HTR case, with similar results qualitatively. The fuel particle undergoes the same three stages, TRISO, BISO, and mono layer coated particle, punctuated by PyC failure. The iPyC layer is seen to break at a fluence of $0.50\times10^{21}$ n·cm$^{-2}$, when the tangential stress at its inner surface surpasses 200 MPa. However, in this case, the oPyC layer breaks at $1.33\times10^{21}$ n·cm$^{-2}$, *i.e.* before the material reaches 30% volumetric swelling. Beyond this point, the SiC layer becomes the sole containment vessel, with its stress evolution governed simply by swelling and creep. The joint action of these two phenomena for a more prolonged time scale results in slightly higher EOL stresses in the SiC layer than for the HTR case. However, the final tangential stresses are of the order of 150 MPa, reasonably well below the SiC strength limit. Times $t_1$, $t_2$ and $t_3$ in Figs. 10 and 11 correspond in this case to, approximately, 0.2, 0.3 and 9.4 years in the LIFE engine.

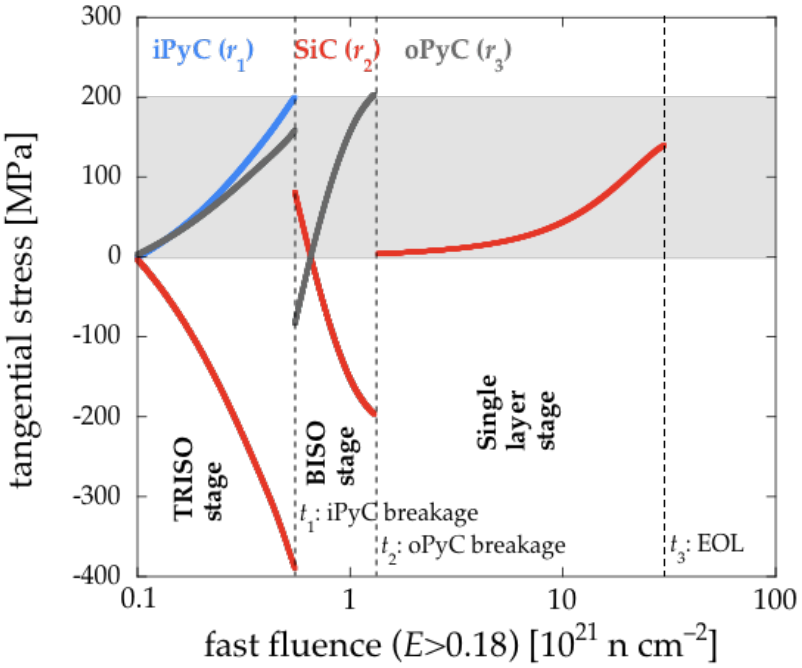


Figure 11: Tangential stress as a function of fast fluence at the inner radii of the iPyC, SiC, and oPyC layers for the DB case. The three vertical dashed lines mark the times at which, respectively, iPyC failure occurs, oPyC failure occurs, and EOL. In the intervals delimited by these times, the fuel particle behaves successively as a TRISO, BISO, and single-layer-coated particle. The shaded region represents the stress regime where PyC retains mechanical integrity.

Incidentally, case (iii) qualitatively represents the expected stress evolution for case (i) if a lower PyC strength were used. As Figure 10 shows, the effect of this early rupture on the overall behavior of the particle is minimal, compared to case (ii).

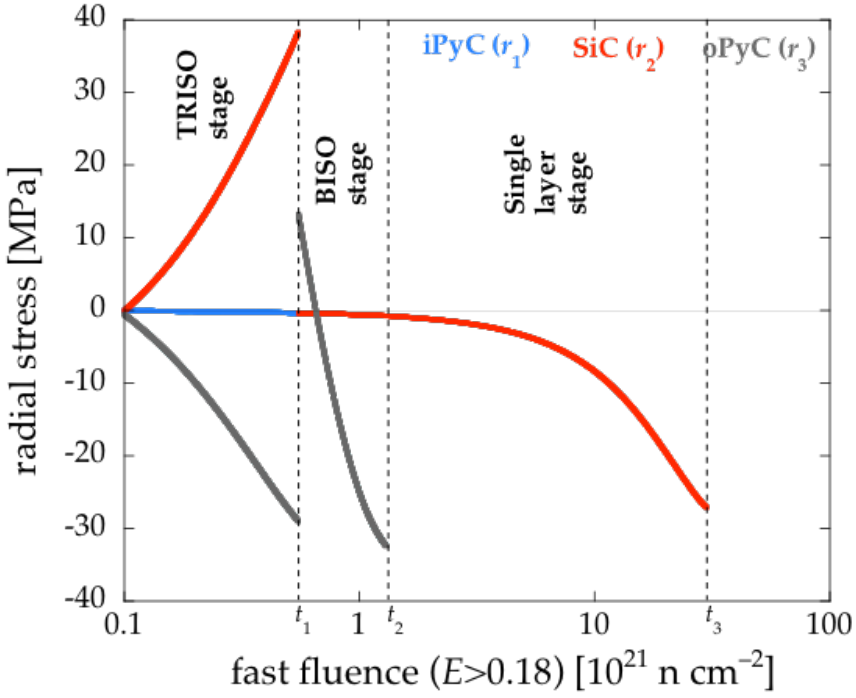


Figure 12: Radial stress as a function of fast fluence at the inner radii of the iPyC, SiC, and oPyC layers for the DB case.

## Graphite pebble behavior

TRISO fuel particles are typically mixed with a graphite powder/phenolic resin paste and pressed into a spherical pebble shape. There are several nuclear grade graphite kinds that have been considered and/or utilized in the context of gas-cooled reactors and fusion reactors. *Gilsocarbon* (polycrystalline) graphite is used in advanced gas-cooled reactors as a moderator and reflector, and its properties at high temperature and fast neutron fluence have been studied in detail [IAEA2000, Li2005, Marsden2005, Marsden2008]. An attractive feature of Gilsocarbon graphite is that, thanks to its intrinsic medium-grained spherical particulate structure, it behaves quasi isotropically[8]. We have opted for this graphite grade for our study and next we consider the behavior of 2-cm-diameter Gilsocarbon pebbles under the LIFE conditions.

The damage and gas[9] production in C in the inner region of the fuel blanket are shown in Figure 13. The procedure used to calculate damage and gas accumulation in materials is given in [Marian2009]. Damage accumulates at a rate of 5.1 dpa per year in the top part of the power curve —thereafter it accumulates at 1.2 dpa per year—, whereas He builds up at 120 appm per year. The reason why He accumulation does not display a slope change is that He transmutation reactions are

[8] With 10 to 20% porosity.
[9] 99.9% He, 0.1% H

caused by fast fusion neutrons that are not affected by burn-up in the fuel blanket[10]. The physical properties for unirradiated Gilsocarbon graphite used here have been compiled from the literature and are summarized in **Table 6**:

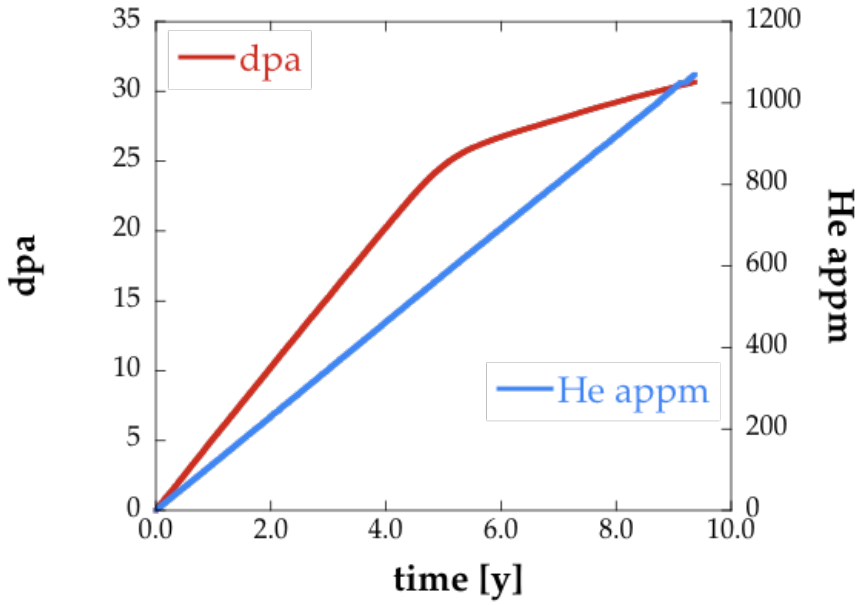


Figure 13: Damage and He accumulation in C in the fuel region of the LIFE engine. The sharp change in slope in the dpa curve corresponds to the power decrease after the fissile inventory has been consumed.

Table 6: Physical properties of unirradiated Gilsocarbon graphite at 700°C.

| | | |
|---|---|---|
| Young's modulus [MPa] | $E_0$ | 10100 |
| Poisson ratio | $\nu$ | 0.11 |
| Poisson ratio in creep | $\nu_c$ | 0.30 |
| Thermal conductivity [$W \cdot m^{-1} \cdot K^{-1}$] | $k_0$ | 80 |
| Thermal expansion coefficient [$K^{-1}$] | $\alpha$ | $4.5 \times 10^{-6}$ |
| Irradiation creep constant [$MPa^{-1} \cdot (cm^{-2})^{-1}$] | $K$ | $2.05 \times 10^{-5}$ |
| Thermal creep constant | $C$ | not available |

[10] (n,α) transmutation reactions in C have a ≈7.0-MeV threshold [ENDF-6], only surpassed by fusion neutrons in LIFE.

| | | |
|---|---|---|
| [MPa$^{-1}$·s$^{-1}$] | | |
| Ideal compressive strength [MPa] | $\sigma_c$ | 75 |

In addition, similar to eqs. (8), the material swells one-dimensionally according to the following law:

$$S(T,\phi t) = \left(s_{21}T + s_{22}\right)\left(\phi t\right)^2 + \left(s_{11}T + s_{12}\right)\phi t$$

which is based on the data by Marsden *et al.* [Marsden2005], and Snead *et al.* [Snead2008]. This relation gives the absolute swelling when $T$ is the absolute temperature and $\phi t$ is the fast fluence (>1.0 MeV) in n·cm$^{-2}$. The constants $s_{21}$=4.3×10$^{-48}$, $s_{22}$=–3.6×10$^{-45}$, $s_{11}$=–2.0×10$^{-26}$, and $s_{12}$=1.4×10$^{-23}$ are fitted to give the appropriate temperature dependence. This linear temperature dependence is valid in the temperature regime where swelling increases with temperature (up to ≈1000°C). Because the gas accumulation in C is not substantial, we have not scaled the swelling law to the LIFE neutron spectrum. The internal temperature is a function of $r$ and is governed, among other things, by the neutron energy deposition per unit volume, $q$, in C in the inner fuel region, which is 130 W·cm$^{-3}$ at full power. However, note that $q$ scales with the power curve as a function of time (Fig. 3) and it is therefore 20.5 W·cm$^{-3}$ at EOL. Finally, the evolution laws for the Young's modulus and the thermal conductivities are, respectively:

$$k(\phi t) = k_0 \exp\left(-1.48\times10^{-21}\phi t\right)$$
$$E(\phi t) = E_0\left[1.5 - 0.5\exp\left(-1.78\times10^{-21}\phi t\right)\right]$$

which are based on existing databases published for irradiated Gilsocarbon [Li2005, Marsden2008]. Here, again, $\phi t$ is the fast (>1 MeV) fluence in n·cm$^{-2}$, $T$ the absolute temperature in K, and $k_0$ and $E_0$ are the unirradiated thermal conductivity and Young's modulus at approximately 700°C (see **Table 6**). As a disclaimer, we must emphasize that these evolution laws were obtained for fast fluences never in excess of 9 dpa, which constitutes about one third of the total dose experienced in the LIFE reactor (see Figure 13). As Boer *et al.* have noted (in Fig. 20 of their article, [Boer2008]), the stress fields of TRISO particles in a graphite matrix on each other are negligible. Consequently, we assume that the contributions of TRISO particles to the overall internal stress state of the graphite pebble are insignificant and we study the temporal stress evolution of an isolated graphite sphere. The solutions to the Cauchy-Euler equation that describes the radial and tangential stresses in an isotropic spherically symmetric solid are:

$$\sigma_r(r) = \frac{7D}{30}\left(r^2 - R^2\right)$$
$$\sigma_t(r) = \frac{7D}{30}\left(2r^2 - R^2\right) \qquad (9)$$

where $R$ is the pebble radius, and $D$ is a fluence (time) dependent constant:

$$D = \frac{2q\left(s_{21}(\phi t)^2 + s_{11}\phi t\right)}{3k\left[\frac{1-\nu}{E} + (K\phi t + Ct)(1-\nu_c)\right]}$$

Equations (9), along with the temperature profile across the pebble, are plotted in Figure 14 at EOL ($t$=9.4 years), which represents the worst-case scenario in terms of fast fluence, $\phi t$=1.6×10$^{22}$ n·cm$^{-2}$ (>1.0 MeV). As it can be seen, from eqs. (9), $\sigma_r(0)=\sigma_t(0)=-\sigma_t(R)$ gives the maximum stresses. During operation, Gilsocarbon undergoes densification up to a fast fluence of 9.4×10$^{21}$ n·cm$^{-2}$. This causes the radial stress to become tensile up to 2.5 MPa. As swelling builds up, and the thermal conductivity and elastic constants degrade with irradiation, $\sigma_r$ becomes compressive again to values of the order of –7 MPa at 4.1 years, or ≈10$^{22}$ n·cm$^{-2}$, which represents the maximum stress withstood by the pebbles throughout the entire burn-up cycle (see Figure 15). Subsequently, the time behavior of $q$ governs the stress evolution in the pebble. $\sigma_r$ rises again coinciding with the drop in thermal power shown in Figure 3, and then peaks at –1.9 MPa. Then, it smoothly decreases once more until a value of –2.6 at EOL.

The compressive strength of Gilsocarbon graphite has been estimated by Preston and Marsden [Preston2006] to be ≈75 GPa, safely above the maximum value achieved in LIFE. The maximum tensile strength of 19 MPa given by these authors is also safely above the maximum tangential stress reached in the pebble (≈7 MPa). Therefore, within the uncertainties of the physical properties used here, Gilsocarbon pebbles are thermo-mechanically stable for the entire duration of the LIFE burn-up cycle. This, together with graphite's intrinsic resistance to corrosion by fluoride molten salts [Rosenthal1972, Keiser1977, McCoy1978, Fukada2002, Goraieb2002] makes graphite fuel pebbles well suited to withstand the conditions in LIFE's WG-Pu fuel blanket for the entire duration of the burn-up cycle.

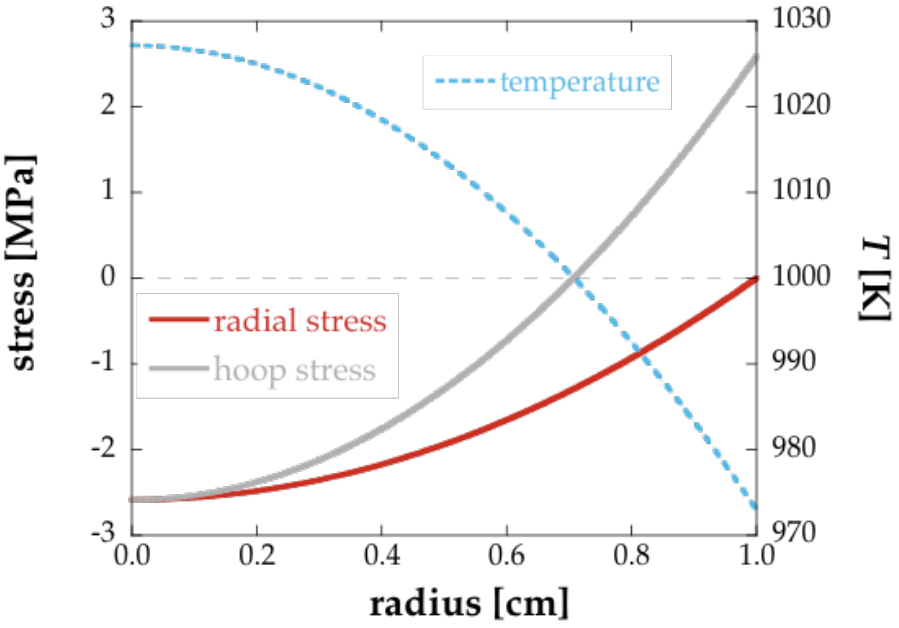


Figure 14: Radial and tangential (hoop) stress at EOL for a 2-cm-diameter graphite pebble. The point of maximum radial stress is located at the center of the particle, whereas the maximum tangential stress is anti-symmetric in [0,*R*]. The temperature profile at EOL is also shown. The surface temperature corresponds to the flibe temperature of 700°C.

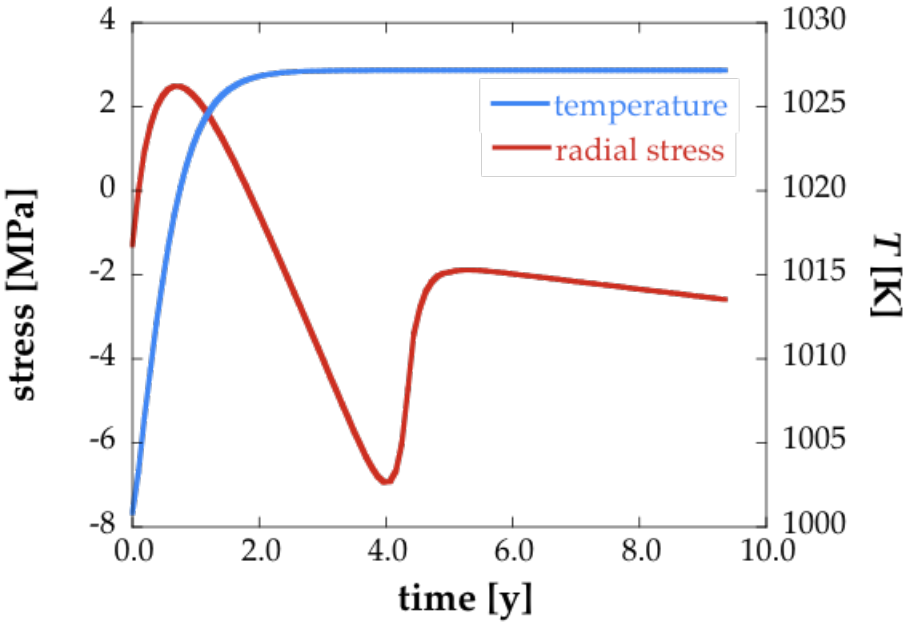


Figure 15: Time evolution over the lifetime of the WG-Pu LIFE engine of the radial stress and the temperature at the center of a 1-cm-radius graphite pebble. The initial densification induced at early fast fluences results in tensile stresses, which become compressive again after approximately two years. After 4 to 5 years, coinciding with the power drop shown in

Figure 3, the radial stress becomes less compressive, after which it settles into a slight increasing steady growth rate until EOL.

## Discussion

It is worth starting by discussing the validity limits of our study, which is carried out in a fast fluence regime that remains unexplored experimentally. Our methodology includes time (fluence)-varying material properties in the form of time correlations that have been fitted to experimental data up to $\approx 4\times10^{25}$ n·m$^{-2}$. Our most radical assumption consists of extending these correlations[11] into the realm of fluences corresponding to the entire LIFE Pu burnup cycle. In cases where the correlations described transient behavior in the experimental regime (e.g. PyC densification), new functional forms were adopted to describe the expected physical behavior into the long-term fluence regimes. With this information, we have developed a methodology that builds on the existing state-of-the-art fuel performance modeling theoretical developments by including (a) time-dependent material properties, (b) yielding (non-rigid) SiC layers, and (c) elastic anisotropy for both SiC and PyC.

Although all our calculations have been performed including all these elements, sensitivity analyses carried out to assess the effect of each of these led to the following conclusions:

(a) Assuming time-varying material properties on SiC and PyC had only a minor effect of the calculated stress evolutions.
(b) Considering a perfectly rigid, vs. a yielding, SiC layer resulted in no appreciable differences in the stress calculations.
(c) Including elastic anisotropy also had a marginal effect on the final results.

With this in mind, the results shown here display a clear sequence of PyC stress buildup and breakage, either by stress overload or by void swelling. This is consistent with the traditional understanding of irradiation effects on TRISO materials. Indeed, Bullock [Bullock1980] indicates that swelling limits the use of PyC to fast fluences of the order of $10^{26}$ n·m$^{-2}$ (>0.18 MeV), which is a third of what is expected in LIFE. For its part SiC is usable up to $10^{27}$ n·m$^{-2}$, safely beyond the burn-up cycle of LIFE's WG-Pu engine. Therefore, PyC swelling alone may suggest extraction of fuel pebbles after 3 years or so of operation (or 8 if our limit of 30% volumetric swelling is used). However, as we have shown, failure of the inner PyC layer does not necessarily imply TRISO-particle failure. For example, Rodriguez *et al.* [Rodriguez2003] have shown that, even in conditions of very high burn-up (>65%), TRISO-particles whose inner PyC layers have failed by chemical attack, debonding, and/or cracking/swelling displayed intact SiC and outer PyC layers, indicating effective retention of fission products. Our results are consistent with this picture, although the stress calculations show that the SiC layer ends up under tangential tension after both the inner and outer PyC layers have failed. Here we

[11] Only when the correlations were not polynomials of degree three or higher. When they were, they were transformed into monotonous functions to avoid unphysical out-of-range oscillations.

have assumed that failure in the PyC —e.g. by crack propagation— does not automatically result in failure of the (adjacent) SiC. This is again qualitatively substantiated by micrographs of failed particles (e.g. [Rodriguez2003]). In our case, while the computed tangential stress in the 'single-layer' regime is always <130 MPa, well below the measured strength of CVD SiC, positive tangential stresses are often taken to be indicative of eventual failure of the SiC layer. Miller *et al.* also observed this phenomenon in simulations of cracked PyC TRISO-coated particles, although their calculated tensile stresses were much larger [INEEL2002b]. In the cases studies, the tangential stress in SiC becomes positive after roughly 1.1 years (at a fluence of $5.46\times10^{25}$ n·m$^{-2}$ —based on case (i) calculations—). We leave to the designer the decision as to whether a moderate level of positive $\sigma_t$ is tolerable or TRISO-coated particles must be subjected to extraction-inspection-recirculation/removal cycles after the calculated fluence limit is reached. Evidently, our method only covers a specific aspect of fuel performance modeling, which, albeit very valuable, is insufficient to enable a fully-informed decision process by the fuel engineer/designer. Other important aspects, not covered here, such as chemical attack modeling, stochastic material property modeling, etc., all or parts of which have been included in some of the codes alluded to in the introduction section, must be considered in unison to develop a truly integrated fuel performance modeling methodology.

In any case, once the SiC layer is directly exposed to the metallic fission products diffusing out of the fuel kernel, it is susceptible of undergoing thinning by chemical attack, which weakens it, leading to premature failure. This is especially important in Pu kernels, where penetration of Pd-Si phases into the SiC layer could be significant in relatively short time scales [Tiegs1982, INEEL2002, Besmann2010]. In this sense, Nosek *et al.* [Nosek2007] have shown that alternative coatings such as TiC or ZrC develop 30% less tangential stresses than SiC while being resistant to chemical attack by metallic fission products. However, these studies lack from sufficient material property irradiation data and are still research concepts. SiC radial stresses stay always below ≈50 MPa, which is likely not sufficient to lead to interfacial debonding according to the experiments of Nozawa *et al.* [Nozawa2007].

The subsequent study of the thermo-mechanical integrity of the graphite fuel pebbles that act as hosts of thousands of TRISO-coated particles has shown that the stresses and temperature gradients developed during the course of a WG-Pu LIFE cycle are sufficiently low to warrant uninspected operation. It is worth noting that, the effect of mutually-interacting TRISO-particles on the stresses has not been considered. However, Boer *et al.* have shown this effect to be small [Boer2008]. Also, although we have simplified the study by choosing a kind of nuclear graphite (gilsocarbon) that displays isotropic mechanical behavior as the subject of our analysis, we do not expect stresses and temperatures to deviate significantly from our results in terms of absolute value for other types of nuclear graphite.

Our methodology is sufficiently general to be applied to other fuel geometries and fuel types. Preliminary work on TRISO-coated fuel with depleted-U-type kernels indicate that the levels of neutron exposure required to achieve ultra-deep burnup in a once-through, closed fuel cycle render the standard HTR-type fuel

based on TRISO-coated particles embedded in graphite pebbles unusable. On the other hand, fuel kernels based on highly-enriched U, Th, or loaded with a sensible mixture of fission products, minor actinides and Pu/Th show a great deal of promise in terms of TRISO suitability and lifetime.

## Conclusions

This work represents a study of TRISO-coated fuel performance modeling in the hybrid LIFE engine with a Pu fuel blanket. Our main conclusions of are:

- We have developed a coupled thermo-mechanical TRISO-fuel performance modeling methodology that includes time and fluence dependent material properties, yielding (swelling and creep) SiC layers, and elastic anisotropy.
- We have applied our method to carry out a numerical study of TRISO particles with two different geometries. Our calculations show that the iPyC layer breaks early in the burnup cycle due to tangential stress accumulation, giving rise to a BISO-like regime with the SiC supporting fission product pressure directly at its inner radius. Subsequently, the oPyC fails either due to stress buildup later on in the cycle or to 30% void swelling. This results in a single-layer (SiC) stage characterized by low tensile tangential stresses.
- We have seen that the influence of the PyC creep coefficient on the overall particle behavior can be significant, and call for more accurate value windows.
- We have calculated the thermo-mechanical evolution of nuclear graphite fuel pebbles, and find that stresses and temperature gradients that develop throughout the entire burnup cycle are tolerable in terms of mechanical and thermal integrity.
- Our analysis shows that TRISO particles in LIFE's WG-Pu hybrid would safely last up to 1.1 years of operation uninspected, or the entire burnup period if a moderate (<130 MPa) level of tensile tangential stress is tolerated.

## Acknowledgments

We would like to thank J. Latkowski, K. Kramer, and J. Powers for providing neutronics data for this study, and S. Zinkle and J. Farmer for helpful discussions. This work performed under the auspices of the U.S. Department of Energy by Lawrence Livermore National Laboratory under Contract DE-AC52-07NA27344.

## Appendix: Calculation of radial and tangential stresses in TRISO layers

Our derivation assumes that the elastic constants are time dependent. Taking the time derivative of the stress-strain equations given by Eq. (1) with the thermal creep exponent $n$=1 gives

$$\dot{\varepsilon}_l = \sum_{m=1}^{3}\left[A_{lm}\sigma_m + B_{lm}\frac{\partial\sigma_m}{\partial t}\right] + \alpha_l\dot{T} + \dot{S}_l(\phi t) \qquad (l=1,3) \qquad \text{(A.1)}$$

where

$$\mathrm{A} = \begin{bmatrix} -\dfrac{\frac{\partial E_1}{\partial t}}{E_1^2} + \dfrac{1}{K_1} + \dfrac{1}{C_1} & \dfrac{\mu_{11}\frac{\partial E_1}{\partial t} - E_1\frac{\partial \mu_{11}}{\partial t}}{E_1^2} - \dfrac{\nu_{12}}{K_1} - \dfrac{\nu_{12}}{C_1} & \dfrac{\mu_{13}\frac{\partial E_1}{\partial t} - E_1\frac{\partial \mu_{13}}{\partial t}}{E_1^2} - \dfrac{\nu_{13}}{K_1} - \dfrac{\nu_{13}}{C_1} \\ \dfrac{\mu_{11}\frac{\partial E_1}{\partial t} - E_1\frac{\partial \mu_{11}}{\partial t}}{E_1^2} - \dfrac{\nu_{21}}{K_1} - \dfrac{\nu_{21}}{C_1} & -\dfrac{\frac{\partial E_1}{\partial t}}{E_1^2} + \dfrac{1}{K_1} + \dfrac{1}{C_1} & \dfrac{\mu_{13}\frac{\partial E_1}{\partial t} - E_1\frac{\partial \mu_{13}}{\partial t}}{E_t^2} - \dfrac{\nu_{23}}{K_1} - \dfrac{\nu_{23}}{C_1} \\ \dfrac{\mu_{13}\frac{\partial E_1}{\partial t} - E_1\frac{\partial \mu_{13}}{\partial t}}{E_1^2} - \dfrac{\nu_{31}}{K_3} - \dfrac{\nu_{31}}{C_3} & \dfrac{\mu_{13}\frac{\partial E_1}{\partial t} - E_1\frac{\partial \mu_{13}}{\partial t}}{E_1^2} - \dfrac{\nu_{32}}{K_3} - \dfrac{\nu_{32}}{C_3} & -\dfrac{\frac{\partial E_3}{\partial t}}{E_3^2} + \dfrac{1}{K_3} + \dfrac{1}{C_3} \end{bmatrix}$$

$$\mathrm{B} = \begin{bmatrix} \dfrac{1}{E_1} & -\dfrac{\mu_{11}}{E_1} & -\dfrac{\mu_{13}}{E_1} \\ -\dfrac{\mu_{11}}{E_1} & \dfrac{1}{E_1} & -\dfrac{\mu_{13}}{E_1} \\ -\dfrac{\mu_{13}}{E_1} & -\dfrac{\mu_{13}}{E_1} & \dfrac{1}{E_3} \end{bmatrix}$$

and $\mu_{32} = \mu_{31}$, $\mu_{23} = \mu_{13}$, and $\frac{\mu_{31}}{E_3} = \frac{\mu_{13}}{E_1}$ was used to eliminate $\mu_{31}$. Power series representations of the strain and stress are assumed. Equations (A.2) cannot be solved analytically for general time-dependent, anisotropic elastic constants. Thus, to obtain a closed-form solution, the coefficients A and B are expanded to second order in time:

$$\mathrm{A} = \sum_{j=0}^{2}\mathrm{A}^{(j)}t^j \qquad \mathrm{B} = \sum_{j=0}^{2}\mathrm{B}^{(j)}t^j$$

Equation (A.1) then becomes

$$i\varepsilon_l^{(i)}t^{i-1} = \sum_{m=1}^{3}\left[A_{lm}^{(j)}t^j\sigma_m^{(i)}t^i + B_{lm}^{(j)}t^j i\sigma_m^{(i)}t^{i-1}\right] + \alpha_l i\dot{T}^{(i)}t^{i-1} + \dot{S}_l^{(i)}t^i \qquad \text{(A.2)}$$

Combining powers of $t$ in each term and shifting the index $i$ so all terms contain the time factor $t^i$ gives

$$(i+1)\frac{\varepsilon_l^{(i+1)}t^i}{r} = \sum_{m=1}^{3}\left[A_{lm}^{(j)}\sigma_m^{(i-j)}t^i + B_{lm}^{(j)}(i-j+1)\sigma_m^{(i-j+1)}t^i\right] + \alpha_l(i+1)\dot{T}^{(i+1)}t^i + \dot{S}_l^{(i)}t^i \qquad \text{(A.3)}$$

Dividing out the factor $t^i$ from each term and solving for $\sigma_m^{(i+1)}$ gives

$$\sigma_m^{(i+1)} = \sum_{k=1}^{3} \frac{C_{km}^{(0)}}{(i+1)\left|\mathrm{B}^{(0)}\right|}\left[\dot{S}_m^{(i)} + (i+1)\left(\alpha_m \dot{T}^{(i+1)} - \varepsilon_m^{(i+1)}\right) + \sum_{l=1}^{3}\left[A_{ml}^{(j)} + B_{ml}^{(j+1)}(i-j)\right]\sigma_l^{(i-j)}\right] \qquad \text{(A.5)}$$

where the $C_{km}^{(0)}$ are the cofactors of $\mathrm{B}^{(0)}$. Equation (A.5) is a recursion relation in which the $(i+1)^{\text{th}}$ stress state is determined by the $(i-j)^{\text{th}}$ stress state, as well as the $(i+1)^{\text{th}}$ expressions for temperature and strain and $i^{\text{th}}$ expressions for swelling and pressure boundary condition. The $(i+1)^{\text{th}}$ terms for the strains $\varepsilon_m^{(i+1)}$ must be determined to obtain the full solutions $\sigma_m^{(i+1)}$ in Eqs. (A.5). This is achieved by applying the elastic equilibrium Eq. (2), thereby eliminating $\sigma_m^{(i+1)}$ in Eq. (A.5) to reduce to an equation in terms of $\varepsilon_m^{(i+1)}$:

$$\sum_{k=1}^{3}\left\{\left[C_{k3}^{(0)}\left(\frac{r}{2}\frac{\partial \varepsilon_3^{(i+1)}}{\partial r} + \varepsilon_3^{(i+1)}\right) - C_{k1}^{(0)}\varepsilon_1^{(i+1)}\right](i+1) + f_{ki}(r)\right\} = 0 \qquad \text{(A.6)}$$

where

$$f_{ki}(r) = C_{k1}^{(0)}\left[S_1 + \alpha_1(i+1)\dot{T} + \sum_{l=1}^{3}\left[A_{1l}^{(j)} + B_{1l}^{(j+1)}(i-j)\right]\sigma_l^{(i-j)}\right]$$

$$-C_{k3}^{(0)}\left[S_3 + \frac{r}{2}\frac{\partial S_3}{\partial r} + (i+1)\left(\alpha_3\dot{T} + \frac{r}{2}\frac{\partial \dot{T}}{\partial r}\right) + \sum_{l=1}^{3}\left[A_{3l}^{(j)} + B_{3l}^{(j+1)}(i-j)\right]\left(\sigma_l^{(i-j)} + \frac{r}{2}\frac{\partial \sigma_l^{(i-j)}}{\partial r}\right)\right].$$

The radial and tangential strains in Eqs. (A.6) are eliminated using the strain-displacement relations [Eqs. (3)] to reduce to a second-order partial differential equation in terms of $u^{(i+1)}$:

$$\sum_{k=1}^{3}\left\{\left[C_{k3}^{(0)}\left(\frac{r}{2}\frac{\partial^2 u^{(i+1)}}{\partial r^2} + \frac{\partial u^{(i+1)}}{\partial r}\right) - C_{k1}^{(0)}\frac{u^{(i+1)}}{r}\right](i+1) + f_{ki}(r)\right\} = 0 \qquad \text{(A.6)}$$

The solutions $u^{(i+1)}$ to Eq. (A.6) are

$$\begin{aligned} u^{(i+1)} &= X_1 r^{p+1} + X_2 r^{q+1} + \sum_{k=1}^{3}\frac{1}{D_k}\left(r^{q+1}\int_{r1}^{r} r'^{-(q+1)} f_{ki}(r')dr' - r^{p+1}\int_{r1}^{r} r'^{-(p+1)} f_{ki}(r')dr'\right) \\ &= \sum_{n=0}^{i+1}(E_n r^{p+1} + F_n r^{q+1})Log(r)^n + \sum_{\tau=-1,\tau\neq 1}^{2} G_{i+1,\tau} r^{\tau+1} \end{aligned} \qquad \text{(A.7)}$$

where $D_k = \dfrac{1}{\sqrt{C_{k3}^{(0)}(8C_{k1}^{(0)} + C_{k3}^{(0)})}}$, $p = \sum_{k=1}^{3}\dfrac{-3C_{k3}^{(0)} + D_k}{2C_{k3}^{(0)}}$, $q = \sum_{k=1}^{3}\dfrac{-3C_{k3}^{(0)} - D_k}{2C_{k3}^{(0)}}$; $X_1$, $X_2$, $E$, $F$, and $G$ are constants determined by applying the boundary conditions and the $r^{\tau+1}$ term arises from the integration of the temperature term (discussed below). It follows that the stresses can be expressed in general form:

$$\sigma_m(r,t) = \sum_{i=0}^{\infty}\sigma_{mi}(r)t^i$$

where

$$\sigma_{mi}(r) = \sum_{j=0}^{i}(H_{mj}r^{p} + I_{mj}r^{q})Log(r)^{j} + \sum_{\tau=-1,\tau\neq 1}^{2} J_{m\tau i}r^{\tau} \qquad \text{(A.8)}$$

$H$, $I$, and $J$ are constants and $p$ and $q$, expressed in terms of the elastic constants by calculating the cofactors of $\mathrm{B}^{(0)}$, are

$$p = -\frac{3}{2} + \frac{1}{2}\sqrt{1 + \frac{8(1-\mu_{13})}{(1-\mu_{11})}\frac{E_1}{E_3}},\ q = -\frac{3}{2} - \frac{1}{2}\sqrt{1 + \frac{8(1-\mu_{13})}{(1-\mu_{11})}\frac{E_1}{E_3}}$$

The temperature profile within the fuel particle is solved from the heat equation,

$$\frac{1}{r^2}\frac{\partial}{\partial r}\left(k(t)r^2\frac{\partial T}{\partial r}\right) - \frac{\partial T}{\partial t} = Q, \qquad \text{(A.12)}$$

with time-dependent thermal conductivity. The solution for $T(r,t)$ in each layer is given by:

$$T(r,t) = \sum_{i=0}^{\infty} T_i(r)t^i = \sum_{i=0}^{\infty}\sum_{\tau=-1,\tau\neq 1}^{2} \mathrm{T}_{\tau i}r^{\tau}t^i = \sum_{i=0}^{N}\left(\frac{\mathrm{T}_{-1i}}{r} + \mathrm{T}_{0i} + \mathrm{T}_{2i}r^2\right)t^i$$

where $\mathrm{T}_{-1i} = -\frac{A_i}{r}$, $\mathrm{T}_{0i} = B_i$, $\mathrm{T}_{2i} = \frac{Q}{6}K_i r^2$, with $A_i$ and $B_i$ constants of integration and $K_i$ is the time series expansion of the inverse of the thermal conductivity. $A_i$ and $B_i$ for the temperature expressions for each layer are found by applying the temperature boundary conditions at the layer interfaces and at the outer surface of the last layer, the values for which are determined from the thermal equilibrium equations.

## References


[abaqus] Abaqus/Standard, version 6.5 used (latest version is 6.9), Simulia Products (http://www.simulia.com/products/abaqus_standard.html).

[Abbott2008] RP Abbott, KJ Kramer, private communication.

[Abbott2009] RP Abbott, MA Gerhard, KJ Kramer, JF Latkowski, KL Morris, PF Peterson and JE Seifried, Fus. Sci. & Technol. 56 (2009) 618-624.

[ATLAS] M Phelip, F Michel, M Pelletier, G DeGeneve, P Guillermier, 2nd International Topical Meeting on High-Temperature Reactor Technology, Beijing, China, Sep 22-24, 2004 (http://www.iaea.org/inisnkm/nkm/aws/htgr/fulltext/htr2004_b03.pdf).

[Bacon1956] GE Bacon, Journal of Applied Chemistry 6 (1956) 477.

[Barnes2008] CM Barnes, DW Marshall, J Hunn, BL Tomlin and JT Keeley, HTR2008-58074, Proceedings of the 4th International Topical Meeting on High Temperature Reactor Technology (HTR2008), Sep 28-Oct 1, 2008, Washington DC, USA.

[Basini2005] V Basini, F Charollais, D Rochais, D Helary, M Perez, P Guillermier, Workshop on Advanced Reactors with Innovative Fuels, ARWIF-2005, Oak Ridge, TN, February 16-18, 2005 (http://www.nea.fr/html/science/meetings/ARWIF2004/3.02.pdf).
[Bennet1991] RG Bennet, Nuclear Technology 96 (1991) 117.
[Besmann2010] TM Besmann, Journal of Nuclear Materials 397 (2010) 69.
[Blackstone1971] R Blackstone and EH Voice, Journal of Nuclear Materials 39 (1971) 319.
[Boer2008] B Boer, AM Ougouang, JL Kloosterman and GK Miller, Nuclear Technology 162 (2008) 276.
[Bongartz1976] K Bongartz, E Gyarmati, H Schuster, and K. Tauber, Journal of Nuclear Materials 62 (1976) 123.
[Bongartz1979] K Bongartz, C2/3, 5th International Conference on Structural Mechanics in Reactor Technology, Berlin, Germany, Aug. 13-17, 1979.
[Brocklehurst1976] JE Brocklehurst and KE Gilchrist, Journal of Nuclear Materials 59 (1976) 7.
[Bullock1980] RE Bullock, Nuclar Engineering & Design 61 (1980) 331.
[CEGA] F Ho, "NP-MHTGR Material Models of Pyrocarbon and Pyrolytic Silicon Carbide", CEGA Corporation, CEGA-002820, Rev 1, July 1993.
[DelCul2002] GD DelCul, BB Spencer, CW Forsberg, ED Collins and WS Rickman, "TRISO-Coated Fuel Processing to Support High-Temperature Gas-Cooled Reactors", ORNL/TM-2002/156, September 2002 (http://www.ornl.gov/~webworks/cppr/y2003/rpt/114586.pdf).
[ENDF-6] http://www.nndc.bnl.gov/exfor/endf02.jsp
[Fukada2002] S Fukada, RA Anderl, Y Hatano, ST Schuetz, RJ Pawelko, DA Petti, GR Smolik, T Terai, M Nishikawa, S Tanaka and A Sagara, Fusion Engineering and Design 61-62 (2002) 783.
[Goraieb2002] AA Goraieb and H Harsch, Fusion Engineering and Design 61-62 (2002) 505.
[Harding2004] J Harding, "Pebble Bed Modular Reactors—Status and Prospects, February 2004 (http://www.rmi.org/images/PDFs/Energy/E05-10_PebbleBedReactors.pdf).
[Heinisch2002] HL Heinisch, LR Greenwood, WJ Weber and RE Williford, Journal of Nuclear Materials 307-311 (2002) 895.
[Homan1978] FJ Homan, PR Kasten and S Peterson, "High-temperature gas-cooled reactor base-technology program", ORNL-5412 (1978).
[IAEA2000] "Irradiation Damage in Graphite due to Fast Neutrons in Fission and Fusion Systems", IAEA-TECDOC-1154, IAEA, Vienna, 2000 (http://www.iaea.org/inisnkm/nkm/aws/htgr/abstracts/abst_xa54410.html).
[IAEA2005] JT Maki and GK Miller, "TRISO-Coated Particle Fuel Performance Benchmark Cases", INL-EDF 3981 Rev 2, March 23rd, 2005.
[INEEL2002] "Development of Improved Models and Designs for Coated-Particle Gas Reactor Fuels", Annual Progress Report Under the International Nuclear

Energy Research Initiative (I-NERI), Nov 2002, INEEL/EXT-02-01493 (http://www.inl.gov/technicalpublications/Documents/2906932.pdf).
[INEEL2002b] GK Miller, DA Petti, JT Maki, "Development Of An Integrated Performance Model For Triso-Coated Gas Reactor Particle Fuel", April 2002, INEEL/CON-01-01553 (http://www.inl.gov/technicalpublications/Documents/3169759.pdf).
[INEEL2004] "Development of Improved Models and Designs for Coated-Particle Gas Reactor Fuels", Final Report Under the International Nuclear Energy Research Initiative (INERI), Dec 2004, INEEL/EXT-05-02615 (http://www.inl.gov/technicalpublications/Documents/3310902.pdf).
[Kaae1971] JL Kaae and JC Bokros, Carbon 9 (1971) 111.
[Kaae1972] JL Kaae, JC Bokros and DW Stevens, Carbon 10 (1972) 571.
[Kaae1974] JL Kaae, Carbon 12 (1974) 577.
[Kaae1975] JL Kaae, Journal of Nuclear Materials 57 (1975) 82.
[Kramer2009] KJ Kramer, JF Latkowski, RP Abbott, JK Boyd, JJ Powers, and JE Seifried, Fus. Sci. & Technol. 56 (2009) 625.
[Keiser1977] JR Keiser, "Compatibility Studies Of Potential Molten-Salt Breeder Reactor Materials In Molten Fluoride Salts", ORNL/TM-5783, May 1977 (http://www.hotfluids.org/references/static/downloads/pdf/ORNL-TM-5783.pdf).
[Lopez2008] E Lopez-Honorato, C Chiritescu, P Xiao, DG Cahill, G Marsh and TJ Abram, Journal of Nuclear Materials 378 (2008) 35.
[Li2005] H Li, BJ Marsden, SL Fok, SMiRT18-W101-9, 18th International Conference on Structural Mechanics in Reactor Technology, Beijing, Chine, Aug. 7-12, 2005.
[Liu2007] B Liu, T Liang and C Tang, Rare Metals 25 (Suppl. 1) (2006) 337.
[Maki2007] JT Maki, DA Petti, DL Knudson and GK Miller, Journal of Nuclear Materials 371 (2007) 270.
[Marian2009] J Marian and M Caro, "Calculation of damage, He and H production using SPECTER", LLNL-TR-416495, 2009 (https://e-reports-ext.llnl.gov/pdf/377654.pdf).
[Marsden2005] BJ Marsden, SL Fok and H Li, SMiRT18-A01-7, 18th International Conference on Structural Mechanics in Reactor Technology, Beijing, Chine, Aug. 7-12, 2005.
[Marsden2008] BJ Marsden, GN Hall, O Wouters, JA Vreeling and J van der Laan, Journal of Nuclear Materials 381 (2008) 62.
[Martin1973] DG Martin, Journal of Nuclear Materials 48 (1973) 35.
[Martin2002] DG Martin, Nuclear Engineering and Design 213 (2002) 241.
[McCoy1978] HE McCoy, "Status Of Materials Development For Molten Salt Reactors", ORNL-TM-5920, January, 1978 (http://www.ornl.gov/info/reports/1978/3445603596348.pdf).
[Miller1993] GK Miller and RG Bennet, Journal of Nuclear Materials 206 (1993) 35.
[Miller1995] GK Miller, Journal of Nuclear Materials 32 (1995) 989.
[Miller2002] GK Miller, DA Petti and JT Maki, Paper 204, 1st International Topical Meeting on High-Temperature Reactor Technology, Petten, The Netherlands, April 22-24, 2002

(http://www.iaea.org/inisnkm/nkm/aws/htgr/abstracts/abst_htr2002_204.html).
[Miller2003] GK Miller, DA Petti, DJ Varacalle and JT Maki, Journal of Nuclear Materials 317 (2003) 69.
[Miller2004] GK Miller, JT Maki, DL Knudson and DA Petti, Paper B20, 2nd International Topical Meeting on High-Temperature Reactor Technology, Beijing, China, Sep 22-24, 2004 (http://www.iaea.org/inisnkm/nkm/aws/htgr/abstracts/abst_htr2004_b20.html).
[Miller2004] GK Miller, DA Petti and JT Maki, Journal of Nuclear Materials 334 (2004) 79.
[Miller2006] GK Miller, DA Petti, JT Maki and DL Knudson, Journal of Nuclear Materials 355 (2006) 150.
[Miller2008] GK Miller, DA Petti, JT Maki and DL Knudson, Journal of Nuclear Materials 374 (2008) 129.
[Morgand1975] P Morgand, Journal of Nuclear Materials 58 (1975) 47.
[Moses2009] EI Moses, T Diaz de la Rubia, EP Storm, JF Latkowski, JC Farmer, RP Abbott, KJ Kramer, PF Peterson, HF Shaw and RF Lehman, Fusion Science and Technology 56 (2009) 547.
[Nickel2002] H Nickel, H Nabielek, G Pott and AW Mehner, Nuclear Engineering & Design 217 (2002) 141.
[Nosek2007] A Nosek, J Conzen, H Doescher, C Martin and J Blanchard, Journal of Nuclear Materials 371 (2007) 288.
[Nozawa2007] T Nozawa, LL Snead, Y Katoh and JH Miller, Journal of Nuclear Materials 371 (2007) 304.
[Phelip2004] M Phelip, Paper B06, 2nd International Topical Meeting on High-Temperature Reactor Technology, Beijing, China, Sep 22-24, 2004 (http://www.iaea.org/inisnkm/nkm/aws/htgr/fulltext/htr2004_b06.html).
[Petti2003] DA Petti, J Buongiorno, JT Maki, RR Hobbins and GK Miller, Nuclear Engineering & Design 222 (2003) 281.
[Powers2009] JJ Powers, "Fuel Performance Modeling of High Burnup Transuranic TRISO Fuels", MS Thesis, UC Berkeley, Spring 2009 (http://www.studentpipeline.org/afci/ms/theses/powers.pdf).
[Prados1967] JW Prados and JL Scott, Nuclear Application 3 (1967) 488.
[Preston2006] SD Preston and BJ Marsden, Carbon 44 (2006) 1250.
[Price1969] RJ Price and JL Kaae, Carbon 7 (1969) 707.
[Rodriguez2003] C Rodriguez, A Baxter, D McEachern, M Fikani and F Venneri, Nuclear Engineering & Design 222 (2003) 299.
[Rosenthal1972] MW Rosenthal, PN Haubenreich and RB Briggs, "The Development Status Of Molten-Salt Breeder Reactors", Oak Ridge National Laboratory, ORNL-4812, August 1972.
[Snead2007] LL Snead, T Nozawa, Y Katoh, TS Byun, S Kondo and DA Petti, Journal of Nuclear Materials 371 (2008) 329.
[Snead2008] LL Snead, TD Burchell and Y Katoh, Journal of Nuclear Materials 381 (2008) 55.
[Talamo2009] A Talamo, Progress in Nuclear Energy 51 (2009) 274.

[Tiegs1982] TN Tiegs, Nuclear Technology 59 (1982) 389.
[Walther1972] H Walther, Nuclear Engineering and Design 18 (1972) 11.
[Wang2004a] J Wang, RG Ballinger and HJ McLean, Nuclear Technology 148 (2004) 68.
[Wang2004b] J Wang, RG Ballinger, HJ McLean and JT Diecker, Paper B20, 2nd International Topical Meeting on High-Temperature Reactor Technology, Beijing, China, Sep 22-24, 2004 (http://www.iaea.org/inisnkm/nkm/aws/htgr/abstracts/abst_htr2004_b20.html).
[Wang2004c] J Wang, "An Integrated Performance Model for High Temperature Gas Cooled Reactor Coated Particle Fuel", PhD Thesis (Massachusetts Institute of Technology, 2004).
[Wu] C Wu, NHC Hwang and YK Lin, Cardiovascular Engineering 2 (2002)49.